REPORT DOCUMENTATION PAGE

AFRL-SR-AR-TR-04-

0538

1. REPORT DATE	2. REPORT TYPE	3. DATES COVERED
01-09-2003	Final Report	30 September 2000 – 1 October 2003

4. TITLE AND SUBTITLE
A Laser Vorticity Probe for the Characterization and Control of Turbulent Boundary Layers

5a. CONTRACT NUMBER

5b. GRANT NUMBER
F49620-01-1-0009

5c. PROGRAM ELEMENT NUMBER

6. AUTHOR(S)
M. Volkan Otugen

5d. PROJECT NUMBER

5e. TASK NUMBER

5f. WORK UNIT NUMBER

7. PERFORMING ORGANIZATION NAME(S) AND ADDRESS(ES)
Polytechnic University
Mechanical and Aerospace Eng.
Six Metrotech Center
Brooklyn, NY 11201

8. PERFORMING ORGANIZATION REPORT NUMBER

9. SPONSORING / MONITORING AGENCY NAME(S) AND ADDRESS(ES)
Air Force Office of Scientific Research
Unsteady Aerodynamics and Hypersonics Program
4015 Wilson Boulevard, Room 713
Arlington, VA 22203-1954

NA

10. SPONSOR/MONITOR'S ACRONYM(S)
AFOSR

11. SPONSOR/MONITOR'S REPORT NUMBER(S)

12. DISTRIBUTION / AVAILABILITY STATEMENT
This report is available to the public without limitations

13. SUPPLEMENTARY NOTES

14. ABSTRACT

A new laser probe for velocity gradients and vorticity measurements is developed and demonstrated. This new technique provides time- and space resolved measurements. The technique is used in turbulent two-stream mixing layers as well as laminar and turbulent boundary layers for the measurement of several velocity gradients and spanwise vorticity. The technique is based on the direct heterodyning on a photo-detector of coherent light scattered from particles in two adjacent locations in the flow. The measurement of any gradient of a given velocity component can be achieved by properly orienting the optical system. Further, a component of the vorticity vector can be measured by using two sets of transmitting and collecting optics, focused at a single location. The time-frozen measurements of $\partial u/\partial y$, $\partial v/\partial x$, $\partial v/\partial y$ in the boundary and mixing layers were carried out using the laser velocity gradient (LVG) probe. Time-frozen measurements of the spanwise component of vorticity were also carried out using the laser vorticity probe (LVP). The measurements demonstrated the viability of the new measurement technique as a research tool. Analyses and several systematic measurements were also performed to determine the data rates, applicability range, and the intrinsic measurement uncertainty associated with the technique.

15. SUBJECT TERMS
Velocity gradient, vorticity, laser probe, turbulent boundary layers

16. SECURITY CLASSIFICATION OF:			17. LIMITATION OF ABSTRACT	18. NUMBER OF PAGES	19a. NAME OF RESPONSIBLE PERSON
a. REPORT	b. ABSTRACT	c. THIS PAGE			Dr. M. Volkan Otugen
Unclassified	Unclassified	Unclassified	UL	60	19b. TELEPHONE NUMBER 718-260-3217

Final Report for
AFOSR GRANT F49620-01-1-0009

A LASER VORTICITY PROBE FOR THE CHARACTERIZATION AND CONTROL OF TURBULENT BOUNDARY LAYERS

Prepared by

M. Volkan Otugen

Mechanical, Aerospace & Manufacturing Engineering Dept.
Polytechnic University
Brooklyn, NY 11201

Prepared for

Air Force Office of Scientific Research
Unsteady Aerodynamics and Hypersonics
4015 Wilson Boulevard, Room 713
Arlington, VA 22203-1954

Program Manager: Dr. John Schmisseur

Table of Contents

	Page
1. Abstract	1
2. Introduction	2
2.1. Motivation and Objectives	2
2.2. Current State-of-the-Art	3
3. Measurement Technique	8
3.1. Measurement Principle	8
3.2. General Optical Configuration	9
4. Experimental Facilities and Optical Setup	13
4.1. Two Stream Mixing Layer Facility	13
4.2. Boundary Layer Facility	14
4.3. Optical Setup for LVG and LVP	14
5. Analysis of Measurement Technique	18
5.1. Data Rate	18
5.2. Measurement Uncertainty	21
5.3. Application of LVG to Hypersonic Boundary Layers	22
6. Measurements in Two Stream Turbulent Mixing Layers	25
6.1. LDV Measurements	25
6.2. Velocity Difference Measurements	26
6.3. Velocity Gradient Measurements	27
6.4. Vorticity Measurements	32
7. Measurements in Boundary Layers	35
7.1. Transitioning Boundary Layers	35
7.2. Turbulent Boundary Layers	45
8. Conclusions	55
9. References	56

1. ABSTRACT

A laser-based probe for the direct, non-intrusive measurement of temporally- and spatially-resolved velocity gradient and vorticity is developed and demonstrated. The optical probes developed were used in turbulent two-stream mixing layers as well as laminar and turbulent boundary layers for the measurement of several velocity gradients and spanwise vorticity. The measurement technique is based on the collection and direct heterodyning of coherent light scattered from particles in two adjacent locations allowing the determination of a velocity gradient. The beat frequency of the heterodyned light gives the difference in the Doppler shift and is proportional to the velocity difference of two points. This frequency is analyzed using a conventional laser Doppler velocimetry (LDV) signal processor (in the present, a burst spectrum analyzer). The angle between the laser beam and the direction of the scattered light determines the measured component of velocity. Therefore, a component of the vorticity vector is measured by using two sets of transmitting and collecting optics, focused at a single location, along with two LDV processors. The technique is non-intrusive, straightforward and relatively inexpensive since it uses standard, off-the-shelf optical and electronic components. It also allows the development of a compact probe with integrated instrumentation. In the present research, the time-frozen measurements of $\partial u/\partial y$, $\partial v/\partial x$, $\partial v/\partial y$ in the boundary and mixing layers were carried out using the laser velocity gradient (LVG) probe. Time-frozen measurements of the spanwise component of vorticity were also carried out using the laser vorticity probe (LVP) which is composed of, essentially, two sets of LVP probes. These measurements demonstrated the viability of the new measurement technique as a research tool. Analyses and several systematic measurements were also performed to determine the data rates, applicability range, and the intrinsic measurement uncertainty associated with the technique.

2. INTRODUCTION

2.1. Motivation and Objectives

A detailed understanding of the flow physics is necessary in the development aerospace vehicles with higher performance and reliability. The flow over air vehicles and through their propulsion systems can exhibit practically all complexities associated with turbulent flows including three-dimensional boundary layers, separation and reattachment, unsteady effects and shock waves. For example, flows through the inlets of airbreathing engines can have shock waves, severe velocity skewness as well as pockets of separation. Each of these can have an adverse effect on the performance of the downstream engine components. In the case of advanced aircraft and weapon systems, the external aerodynamics presents several complex features including unsteady separation and vorticity development. A clear understanding of the fundamental physics involved is necessary in order to develop prediction tools and control strategies of such flows.

In order to study such complex flow phenomena in a testing environment, advanced non-contact measurement techniques need to be employed that can provide time-resolved, local measurements of the basic turbulent flow characteristics and the associated mixing and transport, without disturbing the flow field. The velocity gradient and vorticity are two of such flow properties that can provide a wealth of information on the nature of the flow and, hence, directly contribute to the success of new design concepts. The velocity gradient tensor and the vorticity vector can be considered the defining properties of turbulence, whether in development or in equilibrium. The turbulent fluctuations that are superimposed on a mean flow are essentially caused by the vortical motions of various scales and orientations. The direct, time-resolved measurement of velocity gradients and vorticity can also help identify instabilities in transition and characterize coherent structures in turbulent flows that tend to dominate most shear flows. Vorticity is the fundamental mechanism for turbulent transport, responsible for fluid mixing and drag, which are two main concerns in airframe and engine design. Also, the direct and dynamic measurement of a pertinent local velocity gradient could be used in the detection of turbulent events and hence can be employed in the development of active flow control strategies.

The direct measurement of velocity gradients and vorticity, as it is done in the present research, can provide higher accuracy information faster than those inferred from, say, velocity measurements. High quality and detailed turbulent flow measurements are also needed in order to form an extensive and reliable database which can be used in the development of computer codes that incorporate physics-based mathematical models particularly in the high Reynolds number, compressible flow regime typical of aerospace systems. Further, it can play a fundamental role in improving advanced computational tools such as Large Eddy Simulation (LES) by providing key information on the structure and scales of turbulence in high Reynolds number complex flows.

Despite these advantages, the direct measurements velocity gradients and vorticity have been significantly less common than those of velocity among turbulence researchers due to the limitations in the available measurements methods. Most of the previously proposed vorticity techniques have been based on physical probes which have varying degrees of obtrusiveness. The most commonly attempted velocity gradient (and

by extension vorticity) measurement technique is the one based on thermal anemometry. This method uses multiples of hot-wire sensors to measure velocity components at closely spaced locations in order to obtain the appropriate velocity gradients (velocity strain). The existence of a physical probe in the flow not only disturbs the flow but also is vulnerable in hostile flow environments. These types of probes are unsuitable for application in aircraft and engine research also due to their inability to operate in non-isothermal and multiple species gas flow environments and severe difficulties encountered in compressible flows. Until the present technique, few optical methods have been proposed for the direct measurement of vorticity (or even just velocity gradient). These methods have not met with mixed success since they are typically cumbersome, non-direct (vorticity is inferred from the measurement of other flow properties) expensive and non-dynamic. A popular laser-based non-contact velocity measurement technique is the particle image velocimetry (PIV) which can be applied to the measurement of velocity gradients and vorticity. However, as explained in the next section, this technique also has certain shortcomings in the dynamic measurement of vorticity that is well-resolved in space.

The principle objective of the current research work was to develop and demonstrate a laser probe that improves the state-of-the-art in the non- intrusive measurement of velocity gradient and by extension a component of vorticity and addresses the difficulties and limitations of the methods described above. The current effort was essentially to further exploit the velocity gradient measurement concept that was first proposed by Otugen *et al.* (1998) and later by Yao *et al.* (2001) and to develop and demonstrate a laser velocity gradient (LVG) and vorticity probe (LVP) based on this principle. The sensors provide non-intrusive time-frozen measurements well resolved in space. Since the gradient of velocity is measured directly, it has the potential to provide improved accuracy. As will be discussed in the next chapter, the optical system can be configured such that it can resolve the sign of the velocity gradient and vorticity. Further, the sensors are be applicable to both low-speed and high-speed flows including hypersonic boundary layers. A second objective was to use the LVG and LVP techniques in low Reynolds number ($Re_\theta \sim 1000\text{-}3000$) transitioning an turbulent boundary layers.

2.2. Current State-of-the-Art

The vorticity vector is defined as the curl of the velocity vector and can be expressed in the tensor notation in Cartesian coordinates as

$$\Omega_i = \mathrm{E}_{ijk} \frac{\partial U_k}{\partial x_j}$$

where, E_{ijk} is the alternating tensor and U_k is the velocity vector. Obviously, in order to gain a complete understanding of the instantaneous vorticity field, it is desirable to obtain all nine components of the velocity gradient tensor and the three components of the vorticity field simultaneously. However, in most shear flows of practical interest, usually a single component of the vorticity vector (and, correspondingly a single or a pair of velocity gradients) is dominant over the other two and controls turbulent transport. For example, large scale coherent structures in turbulent jets and mixing layers are typically aligned such that they produce the largest vorticity with an axis normal to the main flow

direction. Hence, a wealth of practical information can be gained by the study of this single component.

Most of the previously proposed vorticity techniques have been based on physical probes which have varying degrees of obtrusiveness. In an earlier attempt, Zalay (1976) and Wigeland *et al.* (1977) used a vorticity indicator which is basically a multi-blade vane connected to a shaft which rotated in the direction of vorticity, through a calibration, presumably giving the magnitude of a vorticity component. This rather crude technique has several drawbacks. It is limited to the measurement of vorticity in the streamwise direction only. It creates a large obstruction in the flow and due to the relatively large vane size, typically has poor spatial resolution. Furthermore, since the probe is mechanical, inertia and frictional resistance can cause underestimation of the vorticity magnitude (Huachen and Shiying,1987). Another method is based on the measurement of pressures at different yaw angles via multiple-prong pitot tubes (Freestone, 1988). This technique has the additional capability of measuring vorticity in directions other than the streamwise, however, it has a rather poor angle of acceptance for velocity and thus is not very reliable for large vorticity values. In addition, this intrusive method has relatively poor spatial and no temporal resolution.

The most commonly attempted vorticity (and velocity gradient) measurement technique is the one based on thermal anemometry. This method uses multiples of hot-wire sensors to measure velocity components at closely spaced locations in order to obtain the appropriate velocity gradients. In one of the earliest attempts Kovasznay (1954) used a four-wire probe to determine the streamwise component of vorticity. The technique was expanded in the following years by several researchers in attempts to improve the accuracy and spatial resolution of the method and to obtain multiple components of the vorticity simultaneously. Foss (1976) developed an array of four wires to measure a single component at a time of the cross-stream components of vorticity. Foss and Haw (1990) later refined the probe design to improve its accuracy and made some measurements in a mixing layer. Klewicki *et al.* (1992) used the same method in an attempt to study the cross-stream vorticity components in a turbulent boundary layer. Eckelmann *et al.* (1977) proposed a five sensor arrangement in order to obtain, simultaneously, the two components of vorticity. Wassman and Wallace (1979), Vukoslavcevic *et al.* (1991), Balint *et al* (1991) and Andreopoulos and Honkan (1996), among others, attempted three component simultaneous measurements of the vorticity vector using various configurations of clusters of hot-wire sensors, the latter three using nine independent wires in groups of three at spatially distinct locations. Hot wire-based vorticity and velocity gradient techniques are comparatively less intrusive that those discussed earlier, however, the existence of a physical probe in the flow not only disturbs the flow but also is vulnerable in hostile flow environments. These types of probes are not quite suitable for application to flows involving non-isothermal and multiple species gas environments as well as compressible and supersonic flows. A comprehensive review of velocity gradient and vorticity measurements using hot-wire anemometry is provided by Wallace and Foss (1995).

Several attempts have been made in order to develop laser-based, non-intrusive velocity gradient and vorticity measurement techniques. Lang and Dimotakis (1982) and Lang (1985) used an LDA to measure two velocity gradients simultaneously and, hence, a vorticity component. Driven by an argon-ion laser, the optical system formed a four-

spot probe volume and each of the two components of velocity were measured at two locations separated approximately 2 mm from one another. This way, an approximate value of the vorticity component was measured. The technique is quite cumbersome as it requires appropriately positioned eight distinct the laser beams and collection of Doppler bursts from four probe volumes which are subsequently analyzed by simultaneously using four detectors and LDA signal processors, all to obtain a single component of the vorticity vector. Agui and Andreopoulos (1994) made certain improvements to this LDA-based method. They reduced the number of laser beams to four by using two elongated probe volumes and collecting signal at two distinct locations in the same long volume. Still, they had to use an argon-ion laser and a set of four detectors and signal processors (burst spectrum analyzers) to obtain the four distinct velocities. Furthermore, the elongation of the probe volume using long focal length transmitting lenses results in large fringe spacings and small number of fringes, adding constraints to the measurement system.

Frisch and Webb (1981) proposed a more direct measurement of vorticity components which involves the illumination by a laser light of specially designed and manufactured plastic beads with mirrors embedded in them. The plane, crystal mirrors in the beads reflect the laser light and the time that takes for each reflected light to travel a small angle predetermined by two slits is measured and related to vorticity. This method, which was later refined by Frisch and Ferguson (1991), provides an improved spatial resolution, however, several severe requirements limit the application of the technique in most practical flow situations. The specially manufactured beads are relatively large ($\approx$25 μm in diameter) and need to be refraction index matched with the working fluid. Moreover, the application of this technique is limited to water (and possibly other liquid) flows and may not present much hope for use in gas flows in the future, particularly in high-speed flows. In another laser-based method, a grid of lines are "written" on a plane in the flow by, for example, Raman excitation (for gas flows) or laser-induced fluorescence (with applications to both gas and liquid flows) and subsequently imaged to determine the distortion of the grid to determine the rate of rotation. This allows for the inference of the vorticity component normal to the imaged plane. The drawback of this approach is that it is complicated requiring expensive equipment to obtain limited and only moderately accurate data. The spatial resolution of the techniques in most cases is relatively poor and, since a time delay is needed between the laser excitation and imaging of the interrogated plane, Taylor hypothesis of "frozen turbulence" has to be invoked.

Particle image velocimetry (PIV) (Adrian, 1991) and holographic particle PIV (Barnhardt *et al.*, 1994; Meng and Hussain, 1995) have also been used to obtain vorticity. In recent years, PIV has gained popularity as a planar, two-component velocity measurement technique and has been applied not only to low speed flows but also to transonic (Wernet, 1997) and supersonic aerodynamics (Otugen, *et al*, 1998). Recent efforts to extend the technique to three-component velocity measurement using a stereoscopic technique have met with success (see, for example, Wernet, 1996). In the PIV technique, two pulses of a laser sheet illuminates a planar section of the flow field with an appropriate time delay and the scattered light from seed particles are imaged on either a photographic film or on a CCD camera. Typically, an auto- or cross-correlation technique is applied to the image to determine the average particle displacement in sub-regions of the image from which, the two components of the velocity are obtained. Once

velocity distribution is obtained, an estimate of velocity gradients and, hence, a single component of the vorticity can be made from the data. Although this technique is quite powerful as a planar velocity imaging, its application as a vorticity probe has certain limitations. First of all, each measurement location is a sub-region of the total image and requires a collection of particles for a valid velocity measurement. This curtails its ability to provide spatially-resolved measurement of vorticity in many applications, particularly, since at least two adjacent sub-regions need to be used to form each velocity gradient. Since multiples of particles are needed even for each time-frozen measurement and the laser energy is spread over a large plane imposes a signal-to-noise ratio limitation that is inherently larger than a single point, single particle technique under similar conditions. This, in turn, leads to the requirement that large, high-energy pulsed lasers be used which not only makes the method more expensive, but reduces the probability of manufacture of compact, integrated probes. Also, the multiple particle requirement in each sub-region of a single measurement adds another constraint on the smallest possible spatial resolution dictated by optical diffraction limit.

Several attempts have been made also to directly measure flow velocity gradients using lasers. For example, Breyer *et al.* (1993) and Kreigs and Staude (1995) proposed a laser-pulsed technique based on speckle pattern analysis. This is a complicated method which depends on pulsed lasers and CCD camera systems. Further, it cannot determine the sign of the velocity gradient. Hanson (1984) explored a light heterodyning method. As in the present technique, he attempted to heterodyne on a detector, the scattered laser light from two distinct particles passing through two adjacent locations. However, the proposed heterodyning process is cumbersome and has several optical limitations; it requires the manufacture of miniaturized spatial gratings and rings with geometries specific to the flow to be studied. Furthermore, this approach also is for time averaged measurements only and the sign of the velocity gradient cannot be determined which limits its use in complex flows.

The technique developed in this research improves the state-of-the-art in the non-intrusive measurement of velocity gradient and vorticity by addressing a number of the difficulties and limitations of the current laser-based methods described above. As described next, it allows for the development of a sensor that can be compact and inexpensive and provide both temporally and spatially resolved vorticity data fast. Unlike most of the laser methods listed above, which infer gradients from velocity measurements, the present technique provides a direct measurement of the velocity differences at adjacent locations thereby improving the inherent accuracy of both the gradient and the vorticity measurement and reducing the number of individual measurements to be performed for the same vorticity information. For a velocity gradient measurement, two beams from a laser and a single frequency processor is needed. For each component of vorticity, only four laser beams and two LDA signal processors are required, significantly reducing the complexity and cost of measurements. Furthermore, since it depends on the passage of a single particle through a focused laser beam, smaller diameter scatteres and lower CW laser powers can be employed for meaningful measurements. As we will discuss in this report, while some of the measurements have been made using an Ar-Ion laser with powers in the order of ~100 mW, some other have been accomplished using a 10 mWatt helium-laser.

In the first phase of the research, the laser velocity gradient (LVG) sensor was designed, built and tested (measuring the transverse gradient of the streamwise velocity, $\partial u/\partial y$) in a small scale two stream mixing layer facility. Next, a second component of LVG was built to form the laser vorticity probe (LVP) and the spanwsie component of the vorticity was measured for a range of flow conditions. The mixing layer facility results are discussed in Section 6. In the second phase of the study, a boundary layer facility was built (closed loop water tunnel) and detailed measurements of $\partial u/\partial y$, $\partial v/\partial x$, $\partial v/\partial y$ as well as the spanwise vorticity were made in the moderate Reynolds number turbulent boundary layers (Section 7). The current research also included analyses and systematic measurements for data rate for LVG and LVP techniques as well as a measurement uncertainty. These analyses and the accompanying measurements are discussed in Section 5.

3. MEASUREMENT TECHNIQUE

3.1. Measurement Principle

The LVG technique is based on the direct measurement of velocity difference of particles at two locations by coherent heterodyning of the scattered laser light form the particles at a detector. This is accomplished by collecting the coherent Mie scattered light from two individual particles using a single set of collecting lenses and coupling them into a single mode optical fiber. The fiber is split into two at the receiving end and allows for the easy combination of the scattered light from two locations colinearly. When the output of the fiber is focused on a photodetector, the beat frequency is easily observed. This frequency carries velocity difference information and is analyzed by an LDA processor, such as a counter processor or a frequency domain spectrum analyzer. (In the present work, most of the measurements were made using a burst spectrum analyzer which is a frequency domain system). Since the distance between the two laser beams is known, $\Delta U_i/\Delta x_j$ can be easily calculated. In order to overcome the ambiguity in the sign of the derivative, one of the beams is frequency shifted by using a acousto-optic modulator (Bragg cell). This way, a zero velocity gradient will result in a beat frequency that is equal to that of the modulator frequency (in the present we used 40 MHz).

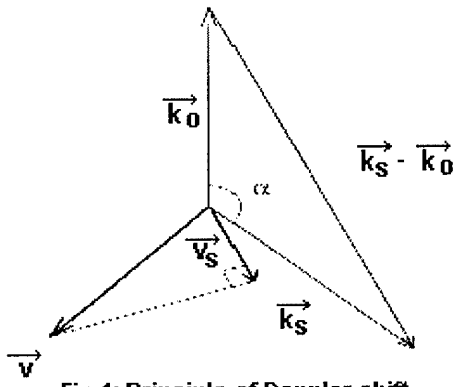

Fig.1: Principle of Doppler shift

Laser light scattered from a moving particle will exhibit a Doppler shift that is dependent on the angle between the incident laser beam and the scattering direction as well as the magnitude of the particle velocity. This principle of light scattering is illustrated in Fig. 1, where $\mathbf{k_0}$ and $\mathbf{k_S}$ (bold face letters indicate vector quantities) are the wave vectors for the incident laser light and the scattered light, respectively. The scattered light from a particle with a velocity of **V** will be Doppler shifted by an amount $\Delta\nu=(1/2\pi)(\mathbf{k_S}-\mathbf{k_0})\cdot\mathbf{V}$. With the assumption that the magnitude of the wave vectors is $2\pi/\lambda$, this shift is expressed by $\Delta\nu=(2V_X/\lambda)\sin(\alpha/2)$ where, λ is the incident laser wavelength and V_X is the component of velocity along the direction $(\mathbf{k_S}-\mathbf{k_0})$. Therefore, by judicially placing the laser beam and the collecting optics, one can select a component of velocity to measure. Also, by changing the magnitude of the angle, α, one can also manipulate the magnitude of the Doppler shift, $\Delta\nu$, to optimize it for a given experiment. In the present LVG technique, scattered light from two closely spaced parallel beams with the same $\mathbf{k_0}$ is collected along a single direction having the same $\mathbf{k_S}$ and heterodyned on a photodetector to directly obtain the difference in Δf. This difference, which is equal to the heterodyne (beat) frequency observed at the detector, is proportional to the velocity difference in x direction (Fig.1).

Now assume the frequency of the scattered light from the two adjacent particles are ν and $(\nu+\Delta\nu)$, where $\Delta\nu$ is the difference frequency, the amplitude at the detector is given by

$$A = A_1 Sin(2\pi\nu t) + A_2 Sin[2\pi(\nu + \Delta\nu)t]$$

Here, A_1 and A_2 represent the signal amplitude from the two scattering locations and t is the time. (Note that the relative phase of the two signals is ignored in the above since it does not influence the outcome). Since the time constant of the detector is much larger than the period of the light wave, it will respond to the time average of the Poynting vector of the field which is simply proportional to the square of the amplitude. Then, using the trigonometric identity, 2Sin(a)·Sin(b)=Cos(a-b)-Cos(a+b), we obtain

$$\langle A^2 \rangle = A_1^2 \langle Sin^2(2\pi\nu t) \rangle + A_2^2 \langle Sin^2[2\pi(\nu + \Delta\nu)t] \rangle - A_1 A_2 \langle Cos[2\pi(2\nu + \Delta\nu)] \rangle + A_1 A_2 \langle Cos(2\pi\Delta\nu t) \rangle$$

where, brackets, < >, denote time averaging over the time constant of the detector. The time average of the first two terms on the right (inside bracket) is ½ while the time average of the third is zero. Then, if the time constant of the detector is smaller than the period of the difference frequency ($1/\Delta\nu$), we will observe a signal at the output of the detector as

$$S = C\left[(A_1^2 + A_2^2)/2 + A_1 A_2 Cos(2\pi\Delta\nu t)\right]$$

where, C is a constant. Thus, the output will possess a bias (dc component) and a sinusoidal component (ac component). The sinusoidal component has the beat frequency,$\Delta\nu$, which is proportional to the velocity difference. Of course, it is desirable to minimize the dc component relative to the amplitude of the ac signal for optimal measurement conditions. A quick observation reveals that this optimal condition is met when $A_1 = A_2$, that is, when the two laser spots at the probe have the same intensity. A strong mismatch in intensity between the two laser spots in the probe volume, will result in a deterioration of the signal-to-noise ratio.

3.2. General Optical Configuration

A generic optical configuration for the measurement of the vorticity component along z direction is shown in Fig. 2 in order to explain the fundamentals of the measurement technique. Note that several perturbations have been made to this optical configuration through our study in order to achieve a more robust and compact measurement system with better signal-to-noise ratios. U and V are the velocity components along x and y directions, respectively. The laser beams and the collection direction that lie on the x-z (red) plane and are denoted by the subscript, 1, measure $\partial U/\partial$ y. (Note that $\mathbf{k_{0,1}}$ represent two parallel laser beams, one of which is 40 MHz frequency shifted through a Bragg cell, and slightly separated from the other in y direction). Similarly, the laser beams and collecting direction that lie on the y-z plane (blue) and denoted by the subscript, 2, measure $\partial V/\partial x$. Again, one of the two laser beams represented by $\mathbf{k_{0,1}}$ is frequency shifted by a Bragg cell and is separated from the other in the x direction by a small amount. Together, $\partial U/\partial y$ and $\partial V/\partial x$ form the vorticity component $\Omega_Z=(\partial U/\partial y)-(\partial V/\partial x)$.

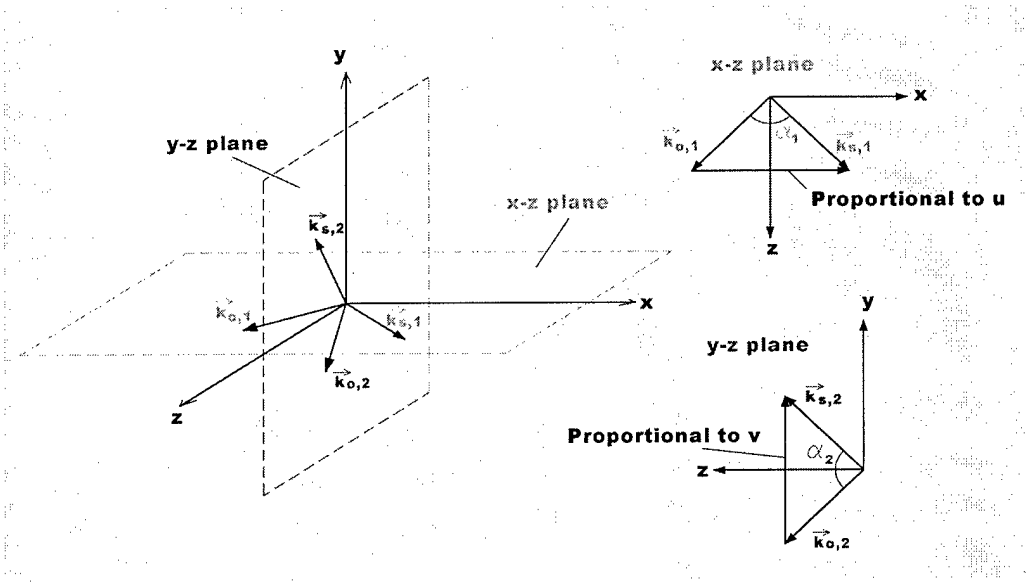

Fig. 2: Optical configuration for the vorticity probe

Figure 3 shows the details of the transmitting and collecting optics for each of the planes. Again, this is a generalized setup drawn to provide an easy explanation. The actual setups used in the present study differ somewhat from that shown in this figure (as will be discussed Section 4). A laser beam is first passed through a Bragg cell. The unshifted and the 40 MHz frequency shifted beams are passed through an iris diaphragm discarding all other higher order beams. A long focal length lens brings the two beams close together at the probe volume where they are nearly parallel. The distance between the two beams is adjustable. The waist of the beams can also be adjusted by telescoping the laser beam ahead of the delivery lens and/or by changing the focal length of this lens. This allows for, if desired, very small spatial resolution on the velocity gradient and vorticity measurement (see Section 4 for details). As an example, a diffraction limit calculation gives a minimum beam waist of about 0.05 mm using a standard He-Ne laser (without having to resort to beam expansion) along with a 100mm focal length achromat. One set of achromatic lenses collect and refocus the scattered light from individual particles on to the ends of two optical fibers. If desired, the focusing lens can have a longer focal length than that of the collimating lens to provide a larger spacing between the pinholes than the two laser beams at the probe. The set of two lights can be separated by a prism as shown and collimated to feed them into the lenses that are attached to the ends of the single mode, polarization preserving fibers. Note that since the single mode fibers have core diameters (in the wavelengths used in the present work) of ~ 4 μm, coupling of the light from the probe into each fiber can be a difficult task. We have investigated several different approaches to optimize the coupling process as will be described later. We use built-in beam combiner to combine the two signals from each fiber. The reason we use optical fiber is (i) ro make the system more compact and rugged and (ii) to obtain the desired colinearity of the two signal beams so that the heterodyne signal can be observed. In order to preserve the coherence and polarization of the two signals (which are needed for the heterodyne process) we

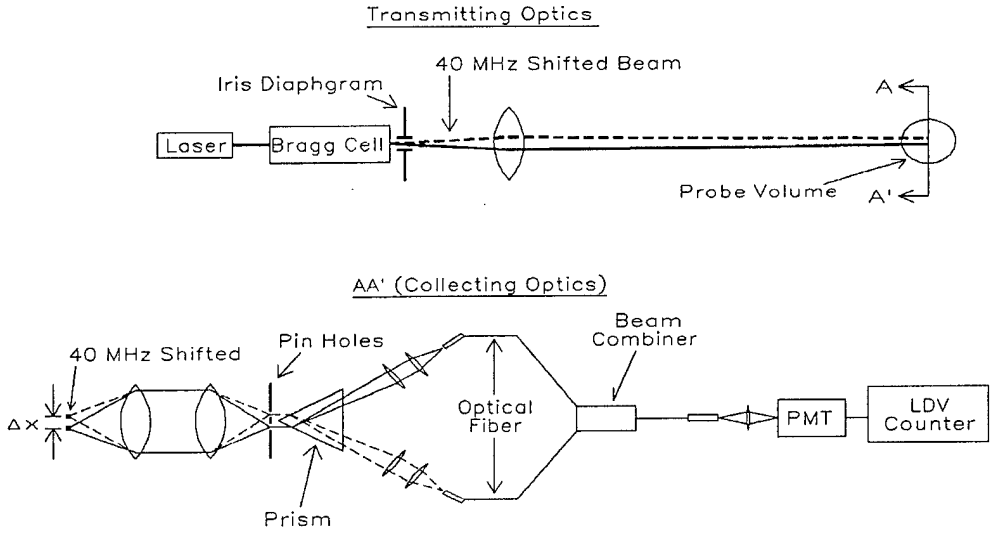

Fig. 3: Optical Setup for the LVG sensor

initially used single mode polarization preserving fibers. A later analysis, however, showed that some multi-mode optical fibers can also be used as long as certain multi mode conditions are met. We carried out measurements using both types of fibers. At the output end of the fiber which contains light from both spots of the probe is another collimating lens. This output is focused onto the surface of a photomultiplier (pmt) tube and the beat frequency, $\Delta\nu$, is observed by a standard LDA processing electronics (tracker, counter or burst spectrum analyzer). The output signal of the processors from each plane (Fig 2) is fed into a PC where the real-time calculation of the vorticity is carried out.

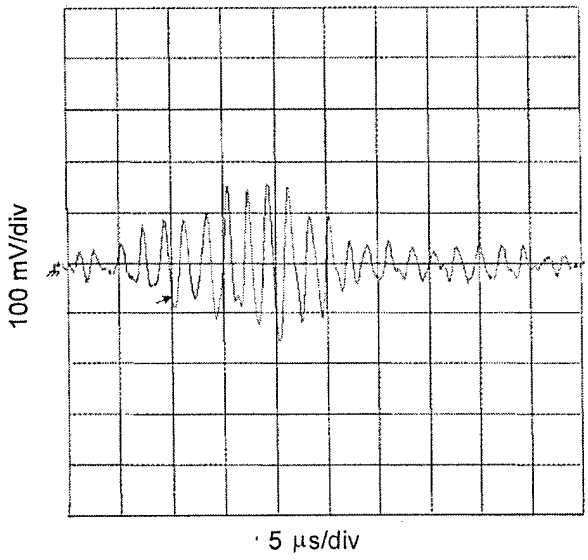

Fig 4: Beat frequency observed on oscilloscope

A sample LVG signal observed on a digital oscilloscope is shown in Fig 4. The signal is conditioned by high- and low-pass filtering to remove the pedestal and high

frequency noise. Clearly, the LVG signal is very similar to the LDV Doppler burst. The only difference is that the frequency of the LVG signal indicates the velocity gradient rather than the velocity of a single location.

4. EXPERIMENTAL FACILITIES AND OPTICAL SETUP

Velocity gradient and vorticity measurements were made using the LVG and LVP techniques in two types of shear flows: turbulent mixing layers and boundary layers. The turbulent mixing layer measurements were made in a small scale water tunnel. Some transitioning boundary layer measurements were also made in this facility. The turbulent boundary layer measurements were made in a larger water tunnel specifically built for this purpose. The details of the two facilities are provided in the next two sections.

4.1. Two Stream Mixing Layer Facility

The two-stream mixing layer facility in which the measurements are made is shown in Fig. 5. It is essentially a small-scale, closed-loop water tunnel whose test section is fitted with a splitter plate dividing the channel into two with equal height (35 mm). The Plexiglas splitter plate is 2 mm thick and is tapered at the trailing edge.

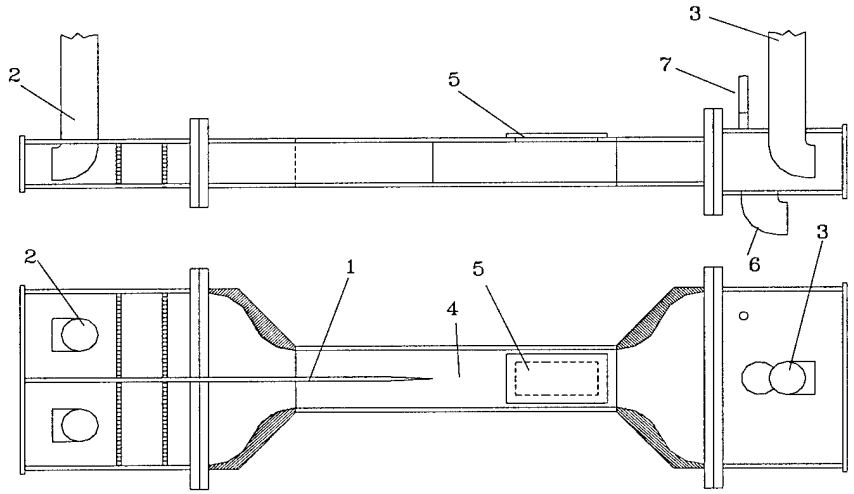

Figure 5: Mixing layer facility [(1)Splitter plate; (2)Inlet; (3)Outlet; (4)Test Section; (5) Access port for probe setup; (6)Drain Pipe; (7)Air Escape]

On the upstream end, the splitter plate extends into the back plate of the plenum completely segregating fluid on each side of the channels so that the velocity in each side of the plate can be controlled independently. Near the upstream end, each side of the plenum contains a perforated plate followed by a set of screens further downstream. The perforated plates serve to make the flow uniform while the combination of different plates and screens allows the manipulation of the turbulence levels in the test section free streams. A pump placed downstream of the diffuser section drives the water flow. The water is discharged into a free-surface reservoir. The velocity of each side is controlled independently via a set of valves upstream of the settling chamber and a bypass loop at the pump. For both the LDV and LVG measurements, the seed particles were introduced into the system at the reservoir. This allows a reasonably well control of the particle loading at the test section. Extensive LDV measurements were made to characterize the

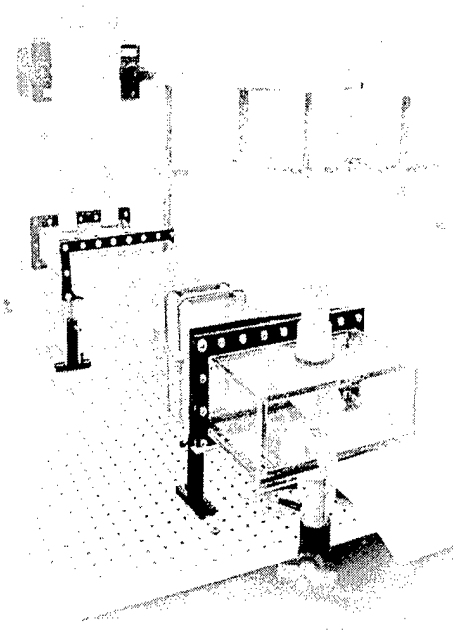

Figure 6: Photograph of mixing layer facility

flow in the test section. Some of these will be presented along with the LVG and LVP results in Section 6. The measurements were made at the mid-span of the test section, upstream at, and downstream of the splitter plate's trailing edge. In the direct velocity gradient measurements (LVG), the probe is aligned such that the transverse gradients of the streamwise velocity were measured.

4.2. Boundary Layer Facility

For the turbulent boundary layer measurements, a larger test facility was used. This facility provides larger and well-characterized turbulent boundary layers. The custom built closed-loop water tunnel facility has a test section that is 2.5 m long and 15.5 cm x 25.5 cm in cross-section. The test section walls provide turbulent boundary layers over smooth surfaces. The test section walls are fabricated from 1.9 mm type SAR clear acrylic Plexiglas. A variable-speed dc motor-driven pump controls the free stream velocity. A maximum free stream velocity of approximately 1 m/s can be achieved in the test section. Turbulent boundary layers with Reynolds numbers of up to $Re_\theta \approx 4500$ can be obtained. The test section is fitted with a moveable segregation wall that can be continuously adjusted (with arbitrary contours) to obtain zero pressure gradient (ZPG), as well as range of favorable pressure gradient (FPG) and adverse pressure gradient (APG) boundary layers. Detailed velocity (LDV) and pressure measurements were carried out to qualify the new facility. Some of these results will be presented in Section 7.

4.3. Optical Setup for LVG and LVP

LVG Probe:

The optical set up for the LVG mixing layer measurements is shown in Fig 7 along with the experimental facility. The optical probe is aligned such that the transverse gradients of the streamwise velocity were measured (see Fig. 8 for the detail of the probe region). For the mixing layer measurements a 10 mW He-Ne laser was used. The laser beam was first passed through a Bragg cell and only the unshifted and +40 MHz shifted beams were allowed to proceed to the test section. The incoming laser beams and the axis of collecting optics were both on a plane normal to the splitter plate. In order to prevent cross talk between the two probe locations, the beams were offset by about 200 μm. The diameter of the laser beams was approximately 200 μm at the probe region. The scattered light from seed particles were collected by a single lens system and subsequently separated by two mirrors and coupled into the two single mode, polarization preserving fibers as shown in Fig 8. (Note that later on during the boundary layer measurements we

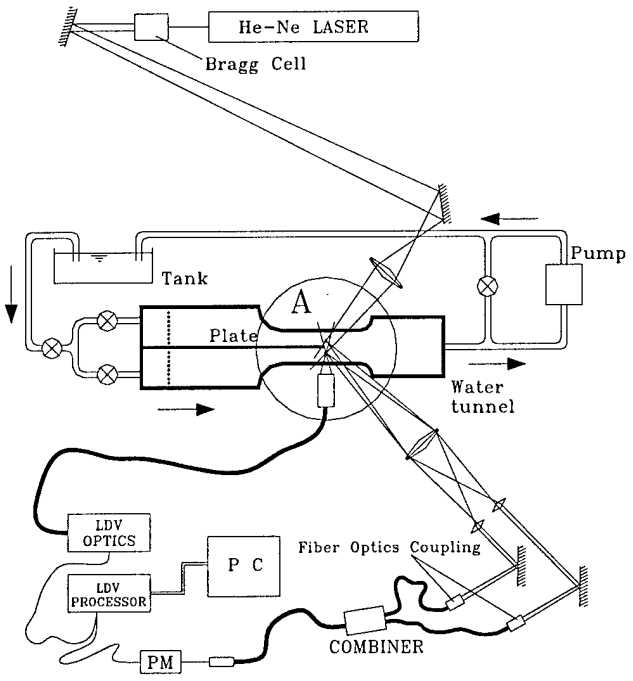

Figure 7: Schematic of water tunnel and the optical system

were able to use a 50 μm core diameter multimode fiber without having to spoil the coherence of the scattered light due to additional fiber modes. The use of a larger core diameter fiber, which essentially acts as a pinhole and defines the probe diameter, not only allows flexibility in choosing the optical probe spot diameter, but also improves the captured signal levels). After combining the signal, the output of one of the fibers is focused onto a photomultiplier tube (PMT). The output of the PMT is fed into a frequency domain processor (LDV burst spectrum analyzer). As indicated in Figs. 7 and 8, simultaneous with the LVG measurements, LDV measurements were also made. From the LDV mean velocity profiles, the mean velocity gradients were calculated and compared with the direct measurements obtained by the LVG.

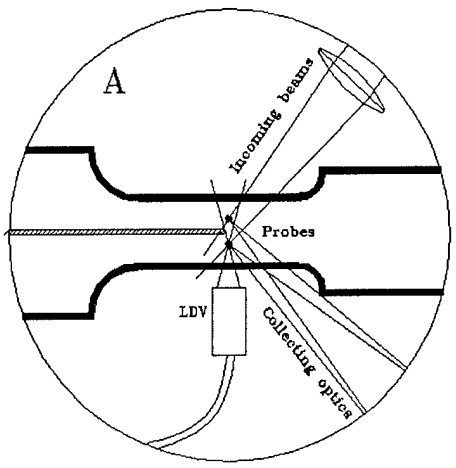

Figure 8: Details of the optical arrangement

Some measurement were also made configuring the optics into a velocity "difference" probe where, the two locations are separated further apart such that they corresponded to the free stream regions (outside of the shear layer). This exercise was carried out in order to critically analyze the particle loading – data rate relation. During these measurements, two additional collecting optics and PMTs are also used to independently track the particle occurrence rate

and velocity on each probe simultaneously with the velocity gradient probe. The single laser spot time-of-flight (L1V) method was used to calculate the velocity in this case (Hirleman, 1987).

LVP Probe:

The optical set up for the LVP vorticity measurements is shown in Fig. 9 and the details of the probe volume are given in Fig 10. The LVP set up is essentially made up of two LVG probes. A single set of transmission optics is used. However, each LVG probe has its own collecting optics and they are situated on the opposite sides of the test section

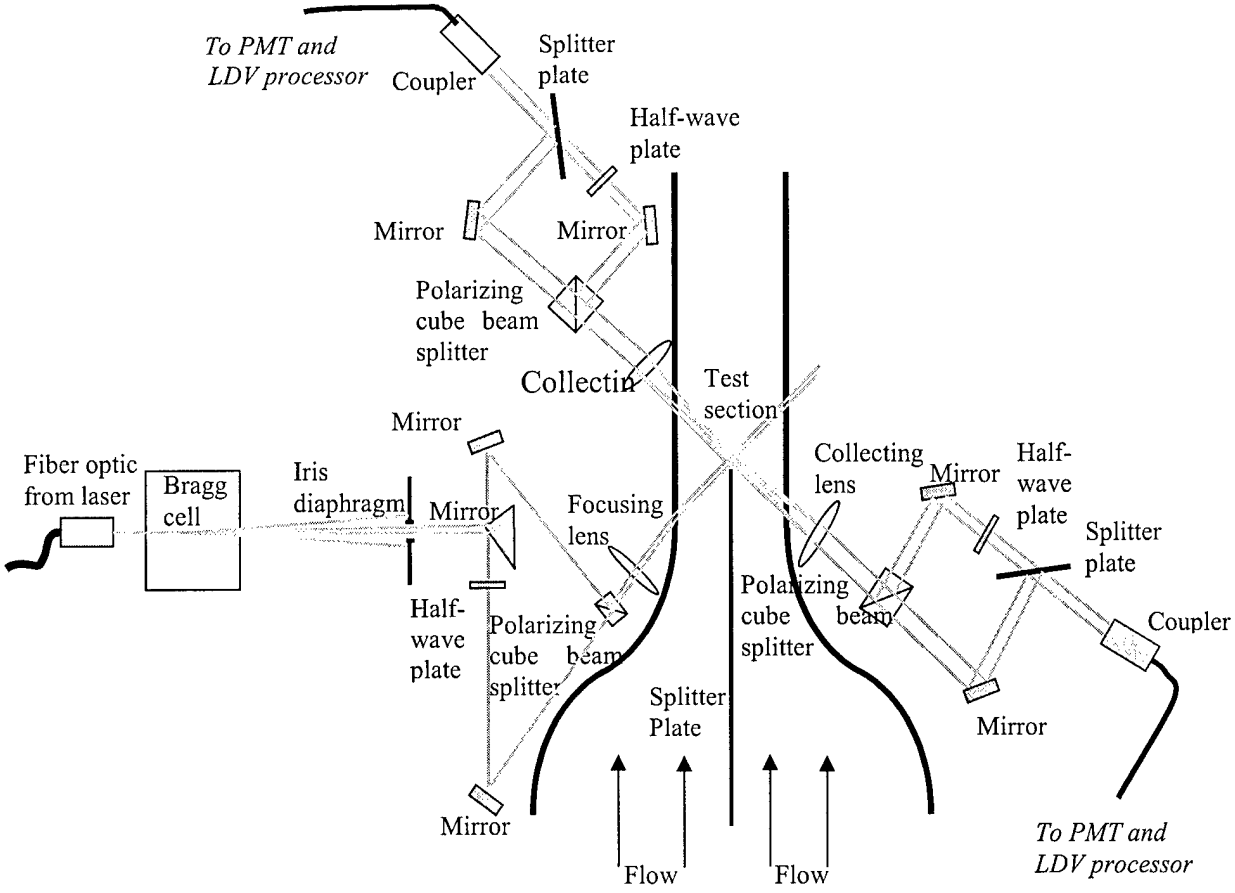

Figure 9: The LVP setup

The probe is aligned such that the spanwise vorticity component is measured (see Fig. 10 for the details). In this configuration, we used an Ar^+ laser. As before, the laser beam is first passed through a Bragg cell and only the unshifted and +40 MHz shifted beams are allowed to proceed to the test section. This time a different method is used to prevent cross talk between the two probe locations. Instead of offsetting the plane of one beam relative to the other, the polarization of one of the beams is rotated 90 deg. The diameter of the laser beams is approximately 180 μm at the probe region. For each of the two

velocity gradients, the scattered light from seed particles is collected by a single lens system and subsequently separated by a polarizing cube beam splitter (which identifies from which laser beam the scattered light comes). An additional half-wave plate is used on one leg to rotate back the polarization (so that heterodyning at the photodetector can take place). The scattered light is then coupled into a 50 μm core diameter optical fiber. The output of each of the fibers is focused onto the PMT (one for each velocity gradient). The outputs of the PMTs are fed into the same two-channel frequency domain processor (LDV burst spectrum analyzer).

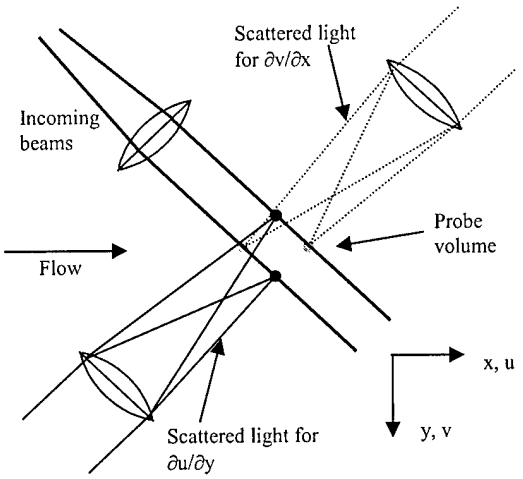

Figure 10: Details o the LVP optical volume

Again, in addition to LVP measurements, LDV measurements were also carried out under the same flow conditions and in the same locations in the flow to characterize the mean velocity and turbulence of the flow. This data is also used to compare with the LVP probe results.

5. ANALYSIS OF MEASUREMENT TECHNIQUE

As part of the study, we carried out analyses to critically assess the viability of the LVG and LVP techniques for a wide range of flows including high-speed compressible boundary layers. Of particular interest were the relationship between data rate and seed particle loading; the intrinsic uncertainty in the proposed measurement technique; and signal-to-noise ratios in high speed flows.

5.1. Data Rate

In order to measure the velocity difference at two locations (the LVG probe), a particle should occur simultaneously at each probe formed by the two laser beams so that a signal with a beat frequency occurs. On the other hand, too many particles at a time in each probe volume will tend to corrupt the coherence of collected light, which will lead to poor light heterodyne. Therefore, particle concentration (loading) plays an important role in both the quality and the rate of data.

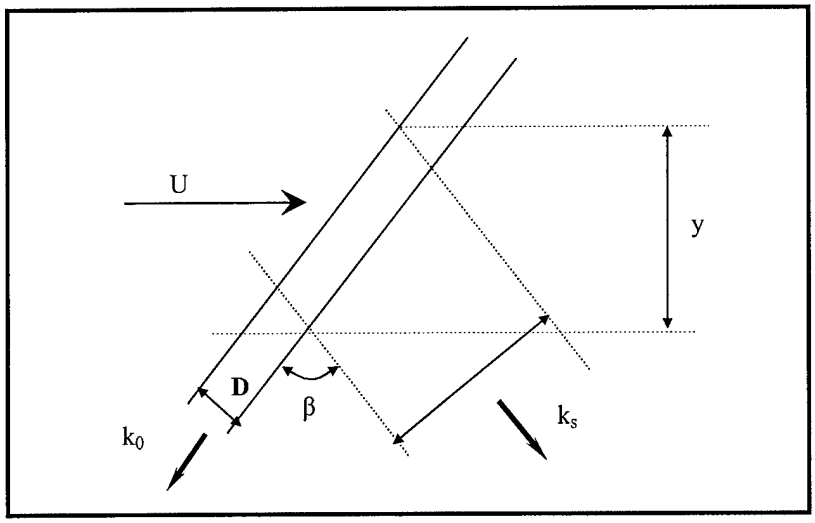

Figure 11: Schematic of a single side of gradient probe

Figure 11 shows one of the two laser beams of the gradient probe with diameter, D, traveling in the $\boldsymbol{k_0}$ unit vector direction. $\boldsymbol{k_s}$ is the unit vector for the scattered light direction. Suppose that the collecting optics look at the section of the beam over the length L, as shown, and the angle between the laser beam and the collection direction is β. U is the mean velocity component as shown. If the particle number density of the fluid is n, the average rate of particle occurrence in the probe volume of Fig. 9 is

$$f_1 = nU\frac{D(D+L)}{2\sin(\beta/2)}$$

For a velocity gradient, we need an additional probe volume located near the first to obtain the gradient and a particle must be present in each of these two probe volumes,

simultaneously, in order to obtain the beat frequency. The time it takes for one particle to traverse one of the two probes is $T_f \approx D/[U\cos(\beta/2)]$. Sometime during this period, a second particle must traverse the other probe volume. Assume that the total time that is required to generate sufficient number of cycles of the beat frequency for a successful velocity difference measurement is T_f/k. This is the coincidental time needed for the particles to be within their respective probe volumes. The value of k will depend on the optical, electronic and flow conditions but, $k > 1$. Then, the average number of particles occurring in the second probe (in sufficient duration) while there is already one in the first probe is given by

$$p_2 = n\frac{D^2(D+L)}{k\sin\beta}.$$

Therefore, the average number of particle occurrence in both probe volumes satisfying the above conditions will be

$$f_{12} = p_2 f_1 = \left(\frac{nD(D+L)}{Sin(\beta/2)}\right)^2\left(\frac{UD}{4kCos(\beta/2)}\right)$$

In the above, f_{12} represents the data rate for a velocity gradient measurement. Note that the average velocity, U is taken to be the same value for both probe volumes. This is a reasonable approach for most flows of interest since for a gradient measurement, the two probe locations must be closely placed and the average velocity difference between the two locations will be small. For highly seeded flows, in order to also consider light extinction through the test section, the number density, n, can be expressed in terms of particle diameter, d, and particle spacing-to-diameter ratio, α as $n=(d\alpha)^{-3}$.

As an example, for a particle loading of $n = 10^{11}$ m^{-3}, probe spot with $L \sim 200$ μm, $D \sim 75$ μm, $\beta = 90$ deg, and a mean flow velocity of $U = 1$ m/s yields a data rate of about ~ 100 Hz for $K = 2$. Higher velocities will yield higher data rates. However, the probe size will have a much stronger impact on the data rate. Larger probe spots will lead to significantly higher data rates. On the other hand, it should be kept in mind that for high Reynolds number flows, the probe spots have to be smaller in order to resolve small-scale turbulent structures. Obviously, a straightforward way to increase data rate is to use high seed densities. However, for highly seeded flows, in addition to the problem of having multiples of seed particles occurring in each probe location, the extinction of the laser light through the test section should also be taken into account. The number density, n, can be expressed in terms of particle diameter, d, and particle spacing-to-diameter ratio, α, as $n = (d\alpha)^{-3}$. As a first order approximation we may assume that extinction takes place only due to particle "blockage" effect. In this case the light intensity, I, can be expressed in terms of particle diameter d, particle loading, n, total distance traveled through the test section, l, and incident light intensity I_0 as

$$I = I_0 e^{(-\frac{n\pi d^2 l}{4})}$$

For the experimental conditions given in the example above, and for l = 10 cm, d = 3 μm, the ratio I/I_0 is approximately 98%. For a more precise model of the particle loading effect on signal quality, several other influences such as multiple scattering and non-zero coefficient of forward Mie scattering may need to be considered.

Experiments were carried out in the two stream mixing layer facility to confirm the above analysis. Of particular interest was the determination of k for the present experimental setup. Table 1 compares the experimentally obtained data rates to those obtained from the analysis for k = *2*. The optical set up was such that each probe was placed in the middle of one free stream so that occurrence of a particle in one probe was statistically independent of the other. Also, seed particle densities were kept small in both channels. In the table, R_1 and R_2 are the number of particles that passed through each probe volume during each measurement. The particle occurrence in each probe is determined simultaneously but independently (of the velocity difference measurement). It is accomplished by detecting and counting particles using an additional set of collecting optics, PMT and data sampling hardware/ software for each probe. n_1 and n_2 are the particle number densities obtained at each probe location using R_1 and R_2. A comparison of the experimental obtained f_{12} to those from the analysis and the relative difference between the two are given in the last three columns of the table, respectively. Keeping in mind that this is essentially an order of magnitude analysis, the agreement between the experiments and the analysis is quite satisfactory.

Table 1: Comparison of Data Analysis with Experimental Results

U_1 (cm/s)	U_1/U_2	R_1 (samples)	R_2 (samples)	n_1 (cm^{-3})	n_2 (cm^{-3})	Tf (ms)	f_{12} (exp.)	f_{12} (theory)	Rel.dif
30.8	1.03	7012	7340	529.31	568.09	0.42	**747**	**720.55**	-3.54
30.8	1.03	3066	2630	231.44	203.55	0.42	**105**	**112.89**	7.51
30.8	1.03	1820	1488	137.39	115.17	0.42	**42**	**37.91**	-9.73
23.0	0.99	900	720	90.86	72.06	0.54	**11**	**11.66**	6.04
23.0	0.99	1476	1206	149.01	120.70	0.54	**29**	**32.04**	10.49
23.0	0.99	2937	3135	296.50	313.77	0.54	**176**	**165.73**	-5.83
39.5	1.90	1215	782	71.52	87.62	0.32	**9**	**10.13**	12.61
39.5	1.90	2676	1680	157.51	188.24	0.32	**44**	**47.95**	8.99
39.5	1.90	6903	3442	406.31	385.67	0.32	**253**	**253.44**	0.17
30.3	1.79	2504	1218	192.14	166.87	0.42	**47**	**42.70**	-9.15
30.3	1.79	3495	1713	268.18	234.69	0.42	**97**	**83.82**	-13.59
30.3	1.79	1615	760	123.92	104.12	0.42	**18**	**17.18**	-4.54

5.2. Measurement Uncertainty

Since only two probe spots are used and that the fact that they are separated by a finite distance results in a first order accuracy. Apart from this, a number of geometric factors contribute to measurement error in determining the velocity gradient. In most applications of LVG, the error in determining the velocity difference will be small and the uncertainty in the distance between the two scattering particles will dominate the measurement error. The error due to the uncertainty in the probe spot separation distance, *dy,* is systematic in nature and will influence the mean value of the velocity gradient. In the present experiments, the estimated relative error in the mean velocity gradient due to this is ± 0.65 % and ± 1.7 %, for the two most commonly used separation distances of *dy* = 770 μm and 300 μm, respectively. The finite size of the probe spots will also contribute to measurement error. The random location of particles in the two probe spots at each measurement will result in the fluctuation of the actual value of *dy* which, in turn, will affect the measured velocity difference and, hence the rms of velocity gradient. Thus, the error in the rms of velocity gradient is a function of probe spot size-to-separation distance ratio, *w/dy* (see Fig 12) and the mean local velocity gradient, $\partial U/\partial y$. Larger values of these parameters will lead to larger rms errors.

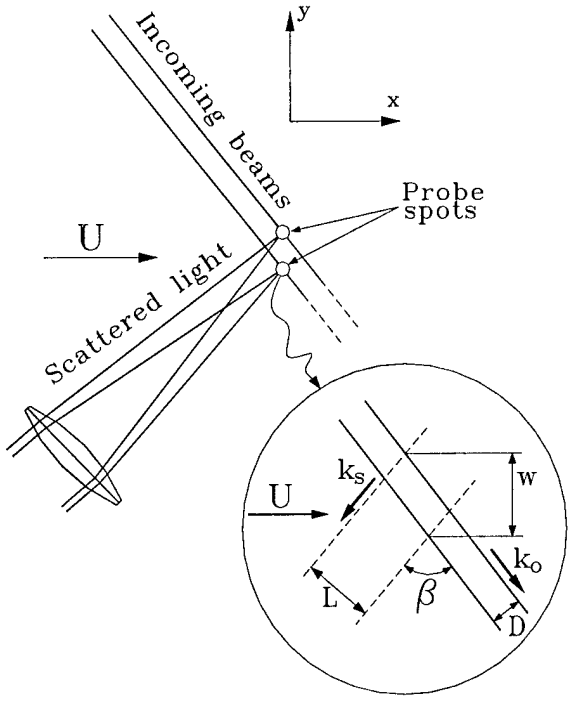

Figure 12: Detail of LVG probe spot

Figure 13 shows the effect of *w/dy* on the rms of the fluctuating velocity gradient. The measurements were made at y = 1 mm from the wall for three boundary layers with free stream velocities U_0 = 0.14, 0.25 and 0.4 m/s. The corresponding $\partial U/\partial y$ values were 51, 108 and 132 s^{-1}, respectively. The range in *w/dy* was obtained by varying both *w* (between 345 and 730 μm) and *dy* (between 300 and 770 μm). Each data point on the figure is determined from 40,000 individual realizations with an average data rate of about 70Hz. For larger *w/dy,* there is significant bias in the measured rms velocity gradient caused by the particle location uncertainty. For *w/dy* < 0.6, the contribution of this "apparent" turbulent velocity gradient on $(\partial u/\partial y)'$ significantly diminishes for all three boundary layers. The figure also shows the effect of the local mean velocity gradient on the measurement error; as pointed out above, larger mean gradients lead to larger bias on the measured $(\partial u/\partial y)'$.

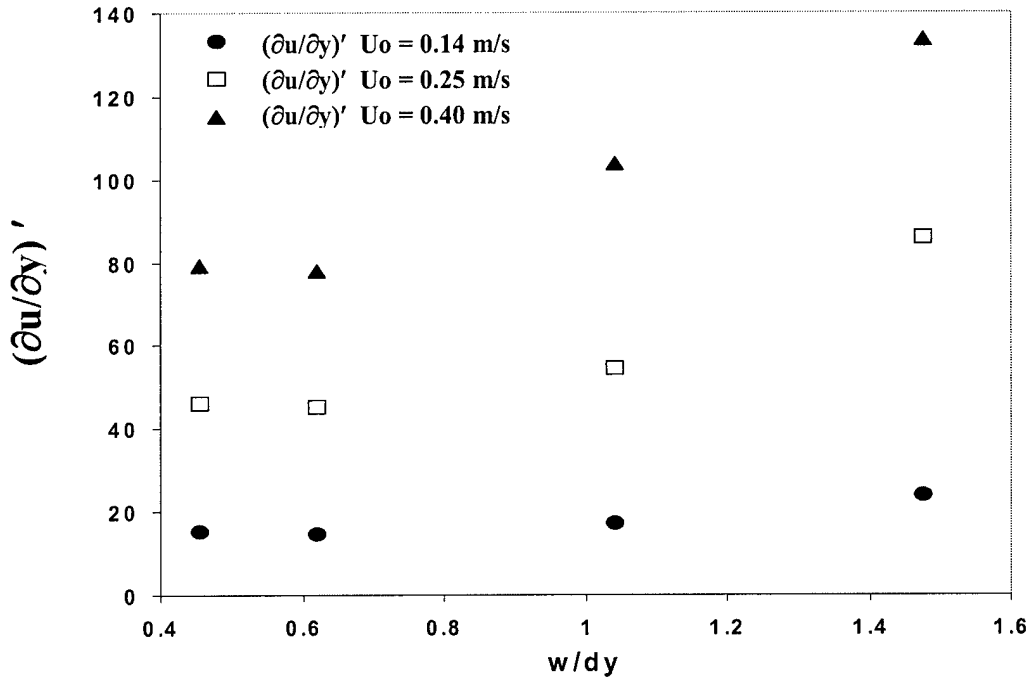

Figure 13: The effect of probe parameter *w/dy* on the rms of velocity gradient

5.3. Application of LVG to Hypersonic Boundary Layers

In this section, we carry out an analysis to determine if the LVG technique can be applied for measurements in hypersonic boundary layers. Of particular interest is the use of wall-mounted sensors based on the LVG principle to measure wall normal velocity gradient in order to monitor near-wall instability and turbulence structures in hypersonic boundary layers. Such sensors would be valuable in the study of instability and transition in such compressible boundary layers. It could also be useful in the development of feedback control schemes for transition delay and separation prevention. In the following analysis we first make an estimate of the flow properties in a typical measurement location inside the boundary layer of a Mach 6 flow at a streamwise station $x \approx 1.25$ m from the origin of the boundary layer. The free stream static temperature and pressure are assumed to be $T_\infty = 100$ K and $P_\infty = 100$ kPa, respectively. The tunnel wall is assumed to be at room temperature.

Magnitude of Streamwise Velocity

The magnitude of the streamwise velocity is important in determining the sensor bandwidth and the heterodyne frequencies that need to be analyzed to determine the velocity gradient. Using the log-law region for a zero pressure gradient incompressible boundary layer, say, at $y^+ = 100$, the streamwise velocity-to-friction velocity ratio is of the order of 17. The incompressible friction velocity is about 30 m/s. The corresponding compressible one at Mach 6 is, then, of the order of 15 m/s. Therefore, if the measurements are made at $y^+ \sim 100$, the streamwise velocity in the region of

measurement will be about 250 m/s. Obviously, higher or lower velocities will be encountered if the measurements are made at larger or lower y^+, respectively.

Number of Cycles per Burst

For low speed flows, using a frequency shift of 40 MHz on one of the incident laser beams, there is always plenty of cycles of the beat frequency as a particle traverses through the probe spot. This may not always be true for very high speed flows where the residence time of a particle in the one of the probe spots may be too small to generate enough cycles of the heterodyne signal. For a streamwise velocity of 250 m/s (as calculated above), if a probe spot size of 100 μm is used, it would take only about $4x10^{-7}$ seconds for a particle to pass through, which is equivalent to a frequency of 2.5 MHz. With a frequency shift of 40 MHz, and a particle that passes through the center of each of the probe beams, we would realize 16 heterodyne cycles for the measurement. For particles passing through off center locations and that are not occurring perfectly coincidentally at two probe spots, the number of cycles would be smaller. Obviously, larger probe spot sizes in the streamwise direction would lead to larger heterodyne burst cycles per measurement. However, bursts composed of as little as four cycles have been successfully processed using this technique. Therefore, the number of cycles generated would be more than sufficient for successful measurements for a probe spot of 100 μm and indeed, smaller probe spots are possible.

Velocity Gradient Range

Here we determine the minimum and maximum velocity difference that can be measured using a wall-sensor based on the present measurement principle. With a given probe separation distance, this gives the range of velocity gradients that the sensor can measure. These values are determined by the optical configuration, the wavelength of the laser diode and the bandwidth of the frequency processor. Our existing frequency domain processors can measure heterodyne frequencies between 4 KHz and 100 MHz. For a wall normal velocity difference, V, laser wavelength, λ, and incident beam-to-collecting direction angle, α, the heterodyne frequency is given by $\Delta f=(2V/\lambda)\sin(\alpha/2)$. For α = 90 degrees, we obtain a minimum and maximum measurable velocity difference of 2 mm/s and 50 m/s. If the two probe spots are separated by a distance of 500 μm, this translates to velocity gradients of $\partial V/\partial x = 4\ s^{-1}$ and $10^5\ s^{-1}$, respectively. We note that the steady, spatially averaged velocity gradient for the hypersonic boundary layer under consideration is $U_\infty/\delta \sim 2x10^5\ s^{-1}$. Therefore, the theoretical limit for the minimum measurable velocity gradient fluctuations is 0.002% of U_∞/δ for the proposed sensor.

Data Rate

As we discussed in Section 5.1, above, a particle has to be present simultaneously at each probe formed by the two laser beams so that a signal with a beat frequency is realized. On the other hand, too many particles at a time in each probe volume will tend to corrupt the coherence of collected light, which will lead to poor light heterodyne. Therefore, data rates may be critical in whether measurements are possible in the near-wall region of hypersonic boundary layers. In the following we use the data rate equations developed in Section 5.1.

For a case of probe spots with L = D = 100 μm and the local streamwise velocity U = 250 m/s estimated above, and taking β = 90 deg. a seed particle number density of n = 10^{12} m^{-3}, gives us a data rate of ~ 3.5 MHz. However, although this particle loading is relatively easy for a well-controlled laboratory experiment, the loading in a large-scale high-speed facility should be expected to be somewhat smaller. A common and relatively simple method to introduce seed particles in the test section of supersonic and hypersonic facilities is by adding humidity into the settling chamber although the method of seeding and its success will depend on the facility and the flow conditions. Generally, the stagnation temperature and pressure will be the determining factor for the seed number density and size. For a given temperature, lower pressures will result in smaller seed particle number densities. On average, a loading of n = $2.5x10^{11}$ should not be unreasonable which gives a data rate of ~2.2kHz. However, for low-pressure hypersonic facilities this number will be smaller. Note that significantly larger data rates can be achieved by increasing the probe spot size by a small amount as indicated in the data rate equation.

Photon Count and Shot Noise

Again, using the numbers developed above, an estimate of the average photon flux can be made. Using a diode laser power of 50 mW, with signal collection solid angle ~ 0.2, avalanche photo diode quantum efficiency ~ 40%, laser wavelength ~ 0.5 μm, scattering angle 90 degrees, and particle index of refraction ~1.5 we will obtain a photon count of N ≈ 10^4 for micron-size particles (using Mie scattering theory). This is for a probe spot diameter of 100 μm and streamwise velocity of 250 m/s (as calculated above). Therefore, the relative shot noise per realization is $(10^4)^{-1/2}$ ~ 1 %. The corresponding shot noise per cycle of a 40MHz heterodyne frequency is about 4.5 %. These values are very reasonable for a frequency domain analyzer.

6. MEASUREMENTS IN TWO STREAM TURBULENT MIXING LAYERS

6.1. LDV Measurements

The LDV measurements were made upstream, at, and downstream of the splitter plate trailing edge to survey the flow for a range of free stream mean velocity ratios, U_1/U_2, before the direct velocity gradient (LVG) measurements. Representative velocity distributions are shown in Figures 14, 15 and 16. These are transverse profiles of the mean and turbulent streamwise velocity obtained at the mid-span of the test section at a streamwise location of x = 4 mm. Both x and y are measured from the trailing edge of the splitter plate and the transverse distance, y, is normalized by the test section half-height, h. Both the mean (solid symbols) and the turbulent (open symbols) velocities are normalized by the maximum mean velocity in each profile. For each velocity ratio of U_1/U_2, a wake region characterized by a mean velocity depression and a turbulence intensity peak is evident. On either side of the wake, a free stream region is evident with a uniform velocity distribution. Note that in all three velocity ratio cases, the free stream turbulent intensity is significant (about 4%). All the measurements were made with a fixed screen/perforated plate arrangement upstream in the plenum chamber which generated a certain turbulence intensity. This screen/perforated plate arrangement was used in order to be able to make velocity "difference" measurements with some level of turbulent

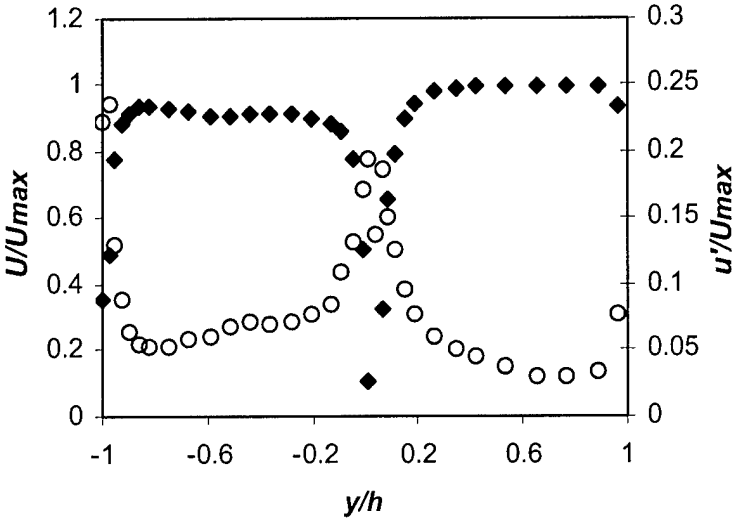

Figure 14: Velocity profile for U_1/U_2 = 0.94

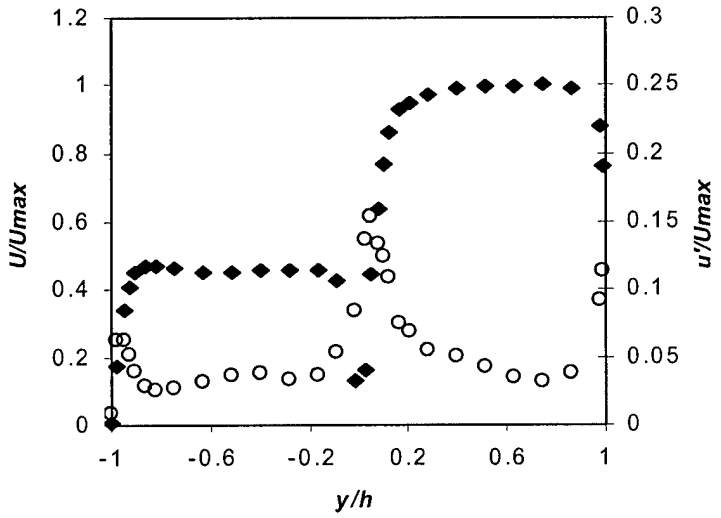

Figure 15: Velocity profile for U_1/U_2 = 0.47

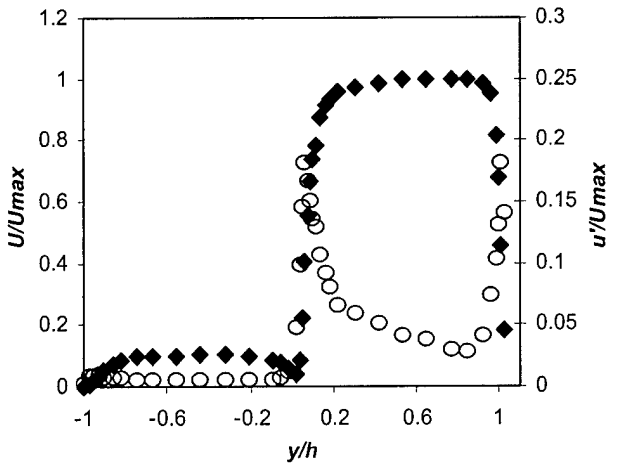

Figure 1 6: Velocity profile for $U_1/U_2 = 0.1$

fluctuations but in the absence of mean shear (as discussed below). Also, in the free stream regions, although the mean velocity gradients are near zero, the turbulent fluctuations generate non-zero rms velocity gradients.

6.2. Velocity Difference Measurements

Prior to embarking upon the LVG measurements, some preliminary velocity "difference" measurements made. In this case, the two measurements spots are separated apart such that they corresponded to the two free stream regions. These measurements were done for two reasons. First of all, for comparison with LDV measurements, this arrangement works out better since it is difficult to accurately position the LDV in the transverse direction. This can lead to measurement errors in the large gradient zone. So for a critical evaluation, the velocity difference configuration provides a better platform. Secondly, it provides a better experimental validation of the particle loading – data rate relation (as was discussed in tprevious section). When the two probes are separated far apart and receive fluid from two different channels, the probability of having a particle in one location is completely independent of particle occurrence in the other location. Therefore this case provides a more critical test for measurement data rate.

Figure 17 compares streamwise mean velocity differences (in the transverse direction) obtained by the current technique with those obtained using the LDV system. The two measurement spots for the velocity difference are at the center of each channel, 35 mm apart from one another. The free stream velocity for each side is varied indep-endently. The solid line in the figure represents the perfect agreement ($y = x$). Clearly, the agreement between the two types of measurements is strong. Note that the same LDV burst

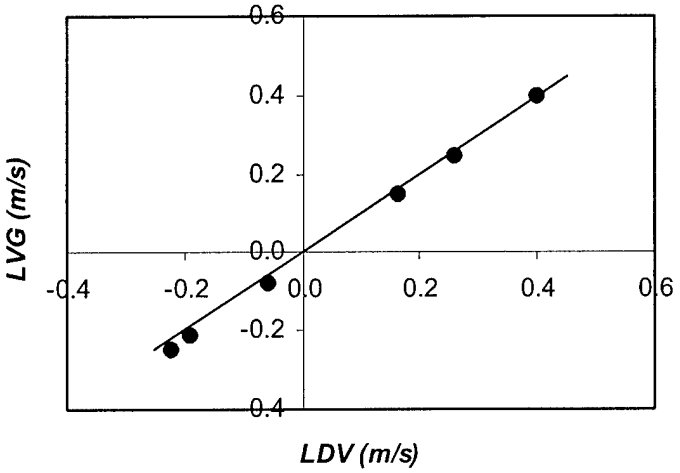

Figure 17: Comparison of LVG and LDV measurements

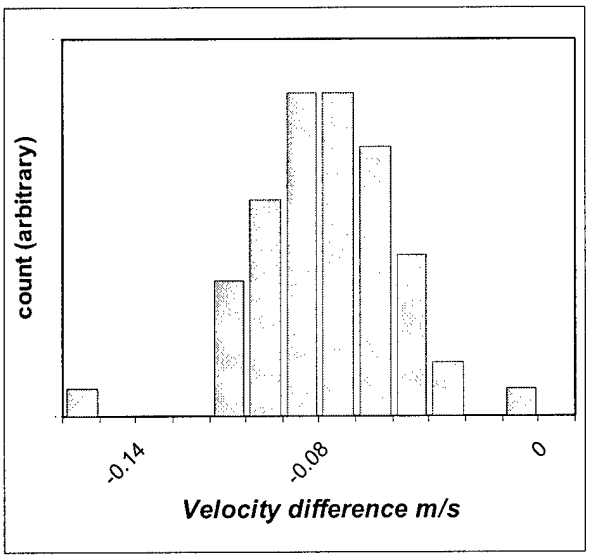

Figure 18: The histogram of LVG record.

spectrum analyzer is used for both sets of data. Data points in the figure represent time-average values (LDV data is the average of approx 5000 samples while the velocity difference data is the average of about 100 samples). Figure 18 is the histogram of a typical LVG record obtained 4 mm downstream of the trailing edge of the splitter plate. The corresponding mean value is – 0.078 m/s. Again, the figure represents the transverse gradient of the streamwise velocity. The flow at this station is turbulent and the streamwise velocity has an rms component. Therefore, the width of the histogram is mainly due to the turbulent fluctuations in the velocity difference at the two locations although it is expected that there is contribution by the system noise. (A statistical analysis indicated that the noise in this preliminary LVG setup is slightly larger than in the LDV). Note that these measurements are made with a He-Ne laser and with the fiber optic system with low coupling/transmission. The next set of LVG results that are presented in the next section below are obtained using a fiber/beam splitter arrangement that improved signal transmission by a factor of about 4.

6.3. Velocity Gradient Measurements

Next systematic measurements of $\partial u/\partial y$ were made in the mixing layer with the two spots of the LVG probe separated by $\Delta y = 300$ μm (with uncertainty of ± 5 μm) in

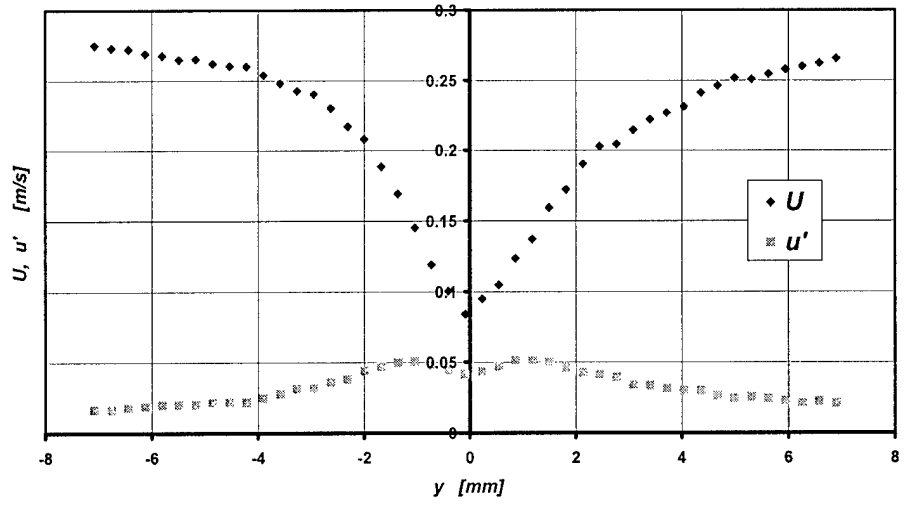

Figure 19: Mean and rms profiles of streamwise velocity in mixing layer ($U_1/U_2 = 1$)

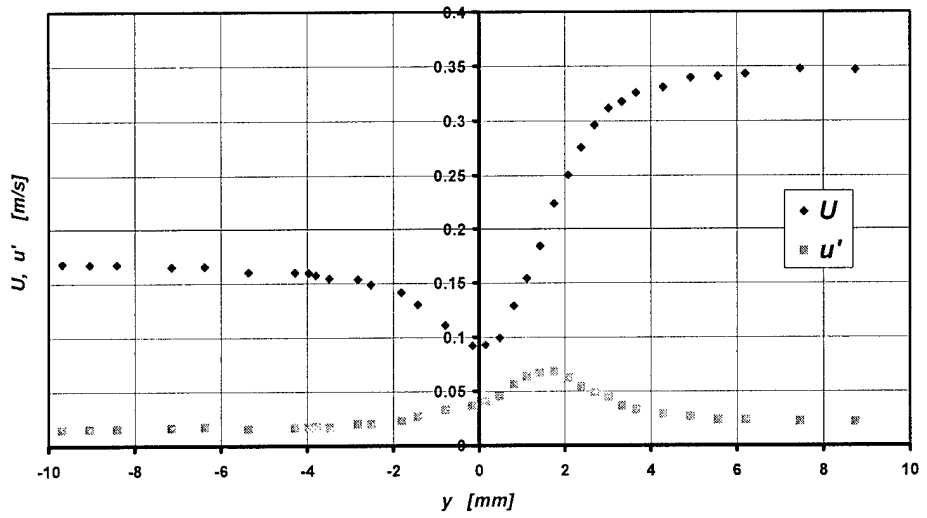

Figure 20: Mean and rms profiles of streamwise velocity in mixing layer ($U_1/U_2 = 0.5$)

the transverse direction. The diameter of each LVG probe spot seen by the collecting optics was ~ 25 μm. Simultaneously, LDV measurements of the streamwise velocity were also made in order to compare the two types of results. The spatial resolution of the LDV probe was approximately 230 μm in the transverse (y) direction. Both the LDV and the LVG optics were placed on the same traverse system to allow for traverses in the y-direction. Again, the two-channel frequency domain signal processor was used to simultaneously analyze the LDV Doppler bursts and the LVG beat frequencies.

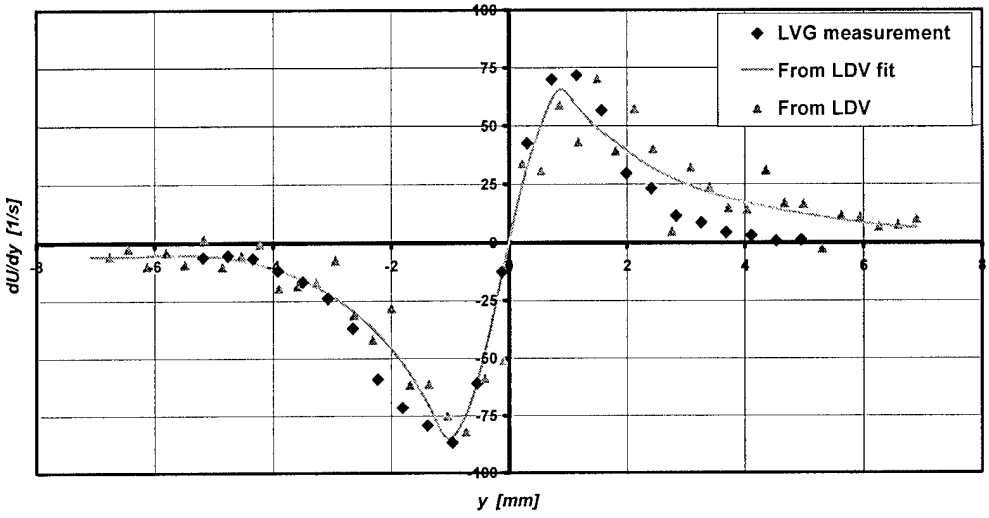

Figure21: Mean velocity gradient profiles in mixing layer for $U_1/U_2 = 1$

Figures 19 and 20 show the transverse distribution of mean and turbulent streamwise velocity in the mixing layer 9 mm downstream of the trailing edge of the splitter plate ($x = 9$ mm) obtained by the LDV system. The free stream velocity ratios are

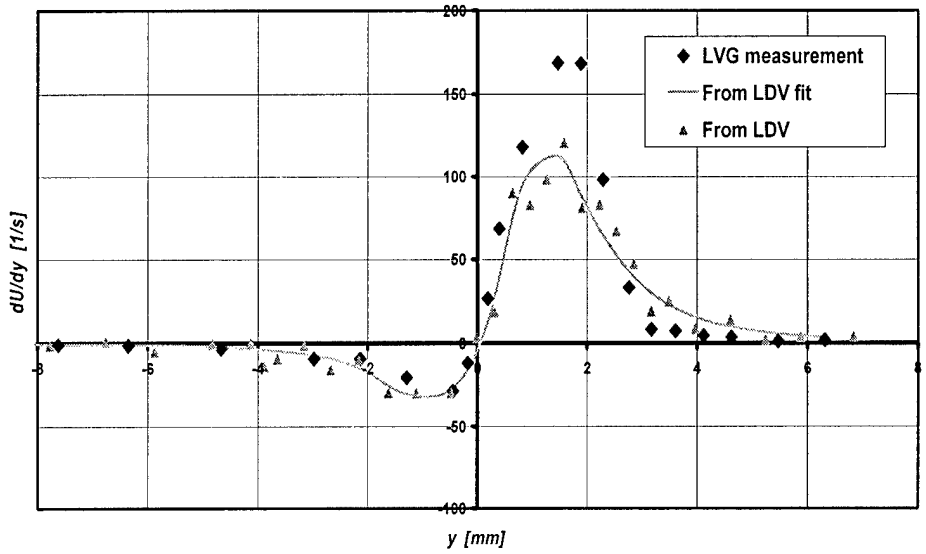

Figure 22: Mean velocity gradient profiles in mixing layer for $U_1/U_2 = 0.5$

$U_1/U_2 \sim 1$ and ~ 0.5 for the two figures, respectively. In the mixing layer with $U_1/U_2 \sim 1$, a maximum of turbulence intensity, u', is observed on each side of the layer roughly corresponding to the location of maximum mean shear while for the $U_1/U_2 \sim 0.5$ mixing layer, only the high mean velocity site of the mixing layer exhibits a maximum in u'. The corresponding mean velocity gradients obtained by the LVG probe are shown in Figs 21 and 22 along with those inferred from the LDV mean velocity profiles. In these two figures, the velocity gradients obtained using the actual LDV data points for the mean velocity profiles (from Figs 19 and 20) show significantly more scatter when compared to the LVG results, clearly demonstrating the reduced uncertainty in this direct measurement. The additional curves in Figs 21 and 22 are obtained by first fitting the LDV velocity profiles with smooth functions and then taking the derivatives of these functions. In general, the agreement is strong between the LVG results and those inferred from the LDV velocity results except that for the $U_1/U_2 \sim 0.5$ case, the maximum mean velocity measured by the LVG method is higher then that calculated from the LDV velocity profile. In any case, these figures clearly show the viability of the LVG technique in turbulent, highly shearing flows.

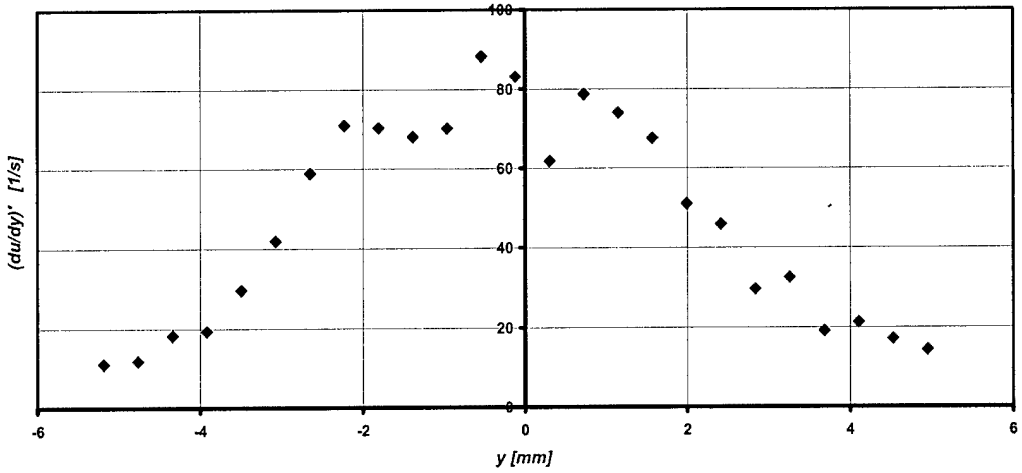

Figure 23; RMS of fluctuating velocity gradient in mixing layer for $U_1/U_2 = 1$

The rms of the fluctuating component of the velocity gradient, obtained from the LVG records is shown in Figs. 23 and 24. The locations of maximum *(du/dy)'* generally coincide with the maximum of the mean velocity gradient. For the $U_1/U_2 \sim 0.5$ case, the

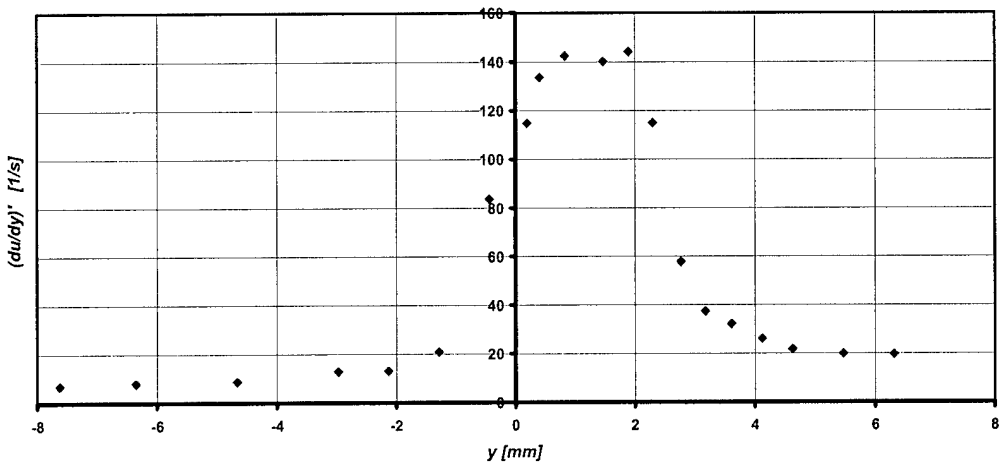

Figure 24: RMS of fluctuating velocity gradient in mixing layer for $U_1/U_2 = 0.5$

maximum of the mean velocity gradient on the low velocity side is too small to generate a maximum of *(du/dy)'*. The approximate values of the relative fluctuation intensity,

(du/dy)' / (dU/dy), at the locations of the maxima are 0.91 and 0.85 for $U_1/U_2 \sim 1$ and 0.5, respectively.

The probability density function (PDF) distributions of the velocity gradient are presented in Figs. 25 and 26. These PDF distributions are among a large number obtained in the present study. As expected, wider distributions are obtained at locations with higher turbulence intensities in the mixing layers. Some skewness in the distributions was

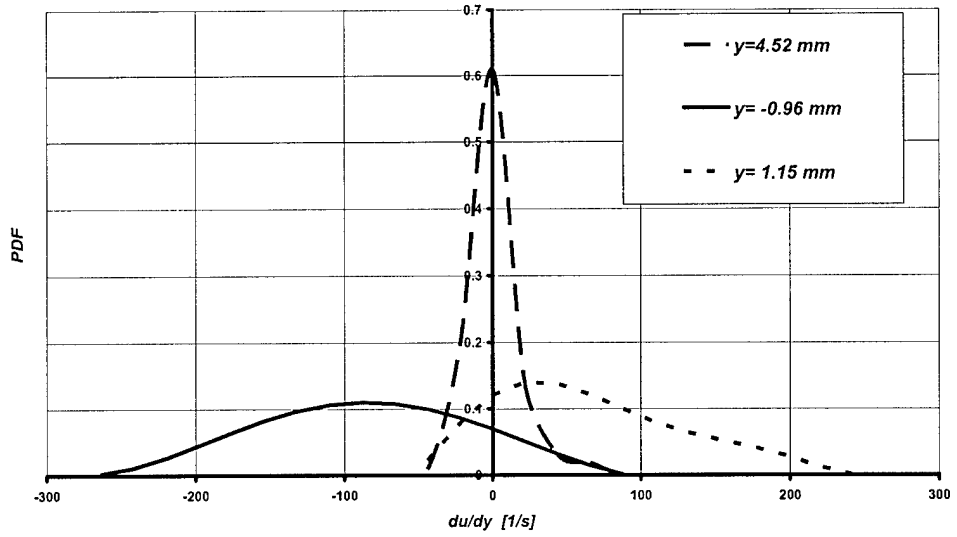

Figure 25: Probability density function of $\partial u/\partial y$ for $U_1/U_2 = 1$

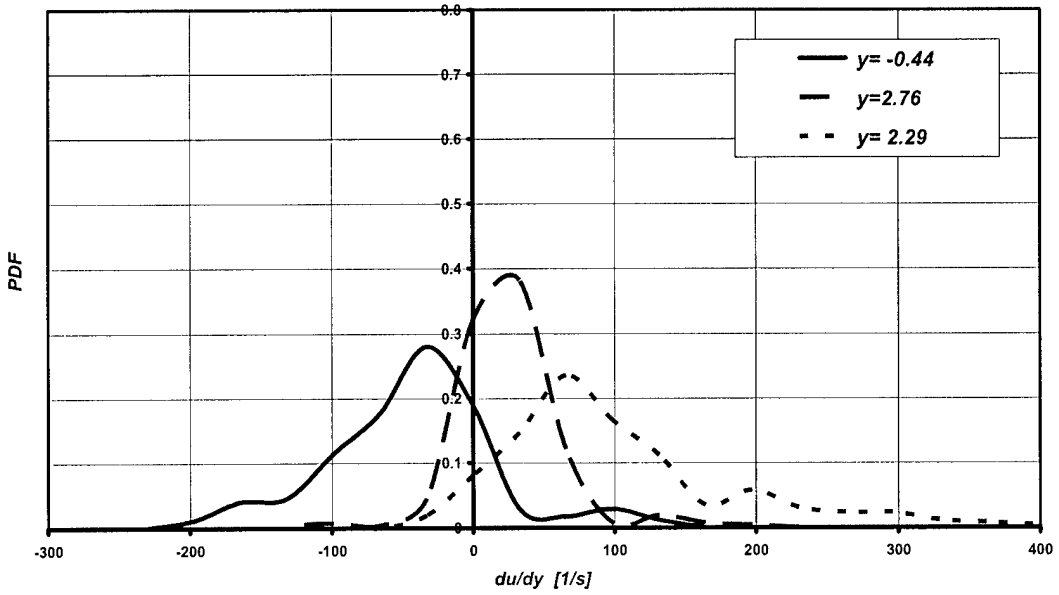

Figure 26: Probability density function of $\partial u/\partial y$ for $U_1/U_2 = 0.5$

also observed near the maximum mean shear locations (see for example y = 1.15 mm in Fig 23). Near the edges of the mixing layers, the distributions became progressively narrow and less skewed. Outside of the mixing layers, the distributions were very narrow and symmetric similar to that obtained for y = 4.52 mm in the mixing layer $U_1/U_2 \sim 1$ (Fig 23).

6.4. Vorticity Measurements

These are the preliminary measurements using the optics as LVP. The measurements were made, again, at the mid-span of the test section and downstream of the splitter plate. Vorticity was measured directly within the shear layer at a single location x = 5.0±0.3 mm and y = 1.7±0.3 mm (the origin is at the trailing edge of the splitter plate). As before, the Ar^+ laser was operated at the 514.5 nm line and delivered a power of about 100 mW to each probe leg. The separation distances for the velocity gradients were ∂y = 1 mm and ∂x = 0.7 mm (See Fig.10). The diameter of the laser beams at the probe region was approximately 180 μm. The collecting optics viewed a region at the laser beams with a diameter of about 200 μm.

In these early measurements the optics were stationary and, thus, the vorticity was measured at a single position but for four different free stream velocity ratios. Flow conditions are summarized in Table 2. U_1 and U_2 are the free stream mean velocities on the two sides of the splitter plate (U_1 corresponds to y < 0 and U_2 corresponds to y > 0).

Table 2: Turbulent Shear Layer Flow Conditions for LVP Measurements

Case	U_1 (m/s)	U_2 (m/s)	U_1/U_2
1	0.27	0.27	1
2	0	0.50	0
3	0.314	0.314	1
4	0	0.593	0

Figure 27 shows the transverse profiles of the mean streamwise velocity, U, for all four cases considered. These profiles were obtained using an LDV system. In the figure y = 0 corresponds to the midpoint of the splitter plate. The profiles were obtained at the streamwise position x = 5 mm behind the trailing edge. The measurement location is close enough to the splitter plate trailing edge to give zero mean streamwise velocity in the splitter plate wake. The LVP measurement location is also shown in the figure. The

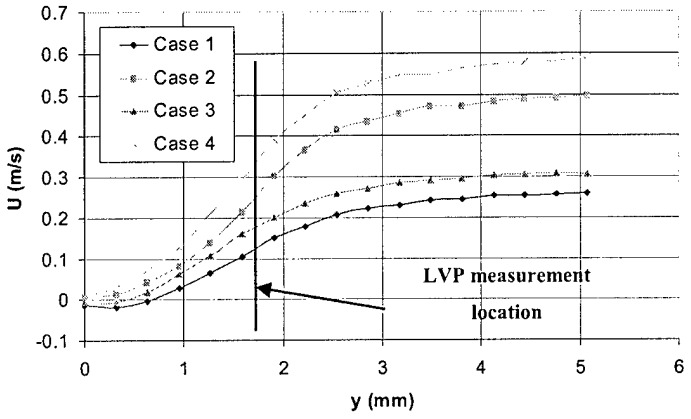

Figure 27: Mean Streamwise Velocity Profiles (LDV)

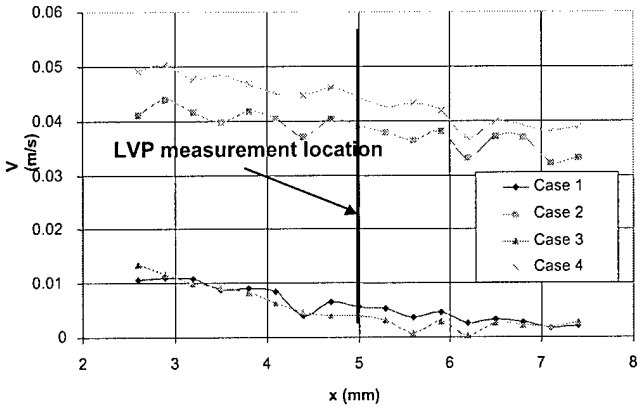

Figure 28 : Mean Transverse Velocity Profiles (LDV)

corresponding mean transverse velocity profiles are shown in Fig. 28. Here, x = 0 is the trailing edge of the splitter plate. The profiles are measured at y = 1.7 mm (below the trailing edge). Comparing Fig. 28 with Fig. 27, it is seen that the magnitude of $\partial U/\partial y$ is much larger than that for $\partial V/\partial x$ indicating that the mean spanwise vorticity will be dominated by $\partial U/\partial y$.

The dissipation per unit volume, ε, and the Kolmogoroff time scale, τ_k, at the LVP measurement location for the four cases studied are presented in Table 3. These are calculated using the LDV results presented above.

Table 3: Turbulent Shear Stress Dissipation Rates and Kolmogoroff Time Scales

Case	ε (m^4/s^3)	Kolmogoroff time scale, τ_k (ms)
1	0.046	4.65
2	0.192	2.28
3	0.051	4.42
4	0.189	2.3

The mean and turbulent vorticity measured by the LVP are presented in Table 4. The mean vorticity results are compared to those calculated from the LDV profiles. The uncertainty values shown for the LVP are calculated taking into account the two dominant sources of error that contribute to the overall error in mean vorticity; (i) the accuracy in determining angle between the laser beam and the collecting angles and, (ii) the accuracy in determining ∂x and ∂y. It is observed that the results determined from the LDV mean velocity profiles are consistently smaller than those measured by LVP. This discrepancy can partially be explained by the limitation in the positioning accuracy of the two sets of probes and the slight change in the flow conditions between the two sets of runs (LDV versus LVP). The turbulent vorticity from LVP was obtained for two different coincidence times for the measured $\partial u/\partial y$ and $\partial v/\partial x$: in one case, the coincidence window is set equal to the local Kolmogoroff time scale and in the other, a longer coincidence time of $\tau = 0.01$ s is used. The average relative discrepancy between the two sets of data is only about 7%.

Table 4: Turbulent Shear Stress Mean and Turbulent Vorticity

Case	ϖ (LDV)	ϖ (LVP)	ω' (LVP) ($\tau = \tau_k$)	ω' (LVP) (τ = 0.01s)
1	-61	-63±9	26	31
2	-109	-140±20	59	61
3	-67	-70±10	40	39
4	-123	-160±30	71	74

Figure 29 shows the probability density function (PDF) of the instantaneous vorticity for the four flow conditions with the Kolmogoroff time scale as coincidence time. For Cases 2 and 4, which have the larger mean and turbulent vorticity values, the PDF distributions are broader. By contrast, these distributions are significantly narrower for Cases 1 and 3.

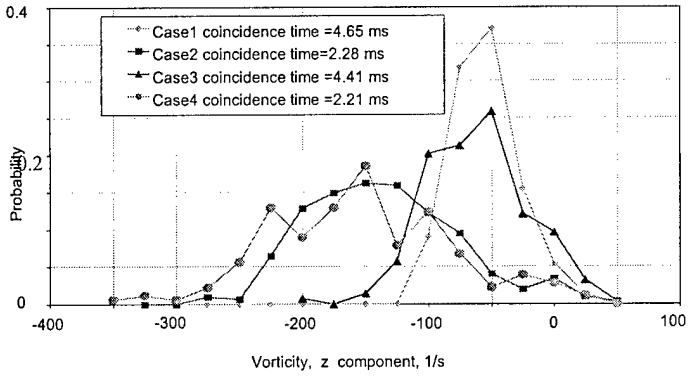

Fig. 29: PDF of Vorticity

Figure 30 compares vorticity PDFs for Case 2 obtained using two different coincidence time windows for $\partial u/\partial y$ and $\partial v/\partial x$ for each realization. The time window τ = 2.28 ms corresponds to the local Kolmogoroff time scale. The figure suggests that the influence of τ on the PDFs in this particular range is very weak. On the other hand, by relaxing the coincidence window requirement to about 4.5 times the Kolmogoroff time scale, the data rate for vorticity is improves by about 3.5 times (from 2 Hz to 7 Hz).

These preliminary measurements indicate that LVP can be applicable to turbulent shear layers and set the stage for more comprehensive measurements in turbulent boundary layers which will be discussed in the next section.

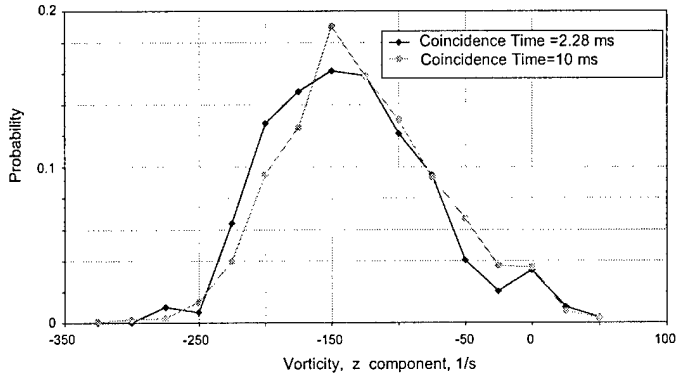

Fig. 30: PDF of Vorticity Measurement from LVP at Different Coincidence Times

7. MEASUREMENTS IN BOUNDARY LAYERS

Two sets of measurements were made; one in transitioning boundary layers and the other in turbulent boundary layers. For the boundary layers in transition, the small scale mixing layer facility was utilized while for the turbulent case, the large-scale boundary layer facility was used.

7.1. Transitioning Boundary Layers

The measurements were made at the mid-span of the test section and at a streamwise location, 33 mm downstream of the splitter plate's trailing edge. The LVG probe was aligned such that the transverse gradient of the streamwise velocity, *du/dy*, was measured. The optical probe was driven by the Ar+ laser. In order to evaluate the effect of probe separation distance on the velocity gradient, measurements were obtained for two separation distances; dy = 770 μm and 300 μm (both, with an uncertainty of ± 5 μm). The diameter of each of the LVG probe spot seen by the collecting optics was ~ 25 μm. In the LVG measurements, the dominant source of error is due to the uncertainty in the actual separation distance between the two particles in each measurement realization (see section 5.2). In estimating the uncertainty for each realization, the size of each probe spot and the scattering particle size have to be taken into account in addition to the uncertainty in the separation distance between the probe spots. In the present, the relative measurement error for a single velocity gradient realization is estimated to be ± 4 % and ± 10 % for dy = 770 μm and 300 μm cases, respectively. However, for mean velocity gradient, this error is only about ± 0.65 % and ± 1.7 %, respectively.

Again, simultaneous with the LVG measurements, LDV measurements of the streamwise velocity were also made in order to compare the two types of results. The single-component LDV system was driven by a 15 mW helium-neon laser and the system was operated in the fully-back scatter mode. The spatial resolution of the LDV probe was approximately 230 μm in the y direction. Both the LDV and the LVG optics were placed on the same traverse system to allow for profile measurements in the y-direction. The same two-channel frequency domain signal processor was used to simultaneously analyze the LDV Doppler bursts and the LVG beat frequency.

Direct measurements of the wall-normal gradient of the streamwise velocity were made in five boundary layers corresponding to the free stream velocities of U_0 = 14, 15.5, 19.5, 25 and 40 cm/s. The profiles were obtained at x = 33 mm. For all the five boundary layers, measurements were carried out with the two spots of the LVG probe separated by dy = 770 μm. Additional measurements were made with dy = 300 μm in the boundary layers with the two highest free stream velocity.

The boundary layer characteristics are summarized in Table 4 where U_0 is the free stream velocity, θ is the boundary layer momentum thickness, H is the shape factor and $\Lambda = -(dP/dx)(\delta^2/\mu U_0)$ is the pressure gradient coefficient. Re_θ is the Reynolds number based on the momentum thickness whereas Re_x is that based on the streamwise distance measured from the beginning of the layer, in this case taken as the location of the straight section of the wall. Although the free stream velocities and Re_x for all the boundary

Table 4: Properties of the boundary layers studied

	U_o (m/s)	δ (m)	θ (m)	Re_θ	Re_x	H	Λ
BL1	0.14	0.0045	0.00060	107	28021	2.15	-
BL2	0.155	0.0042	0.00049	95	30605	2.35	5.00
BL3	0.195	0.0038	0.00047	114	38159	2.33	5.80
BL4	0.25	0.0032	0.00035	109	49464	1.89	-
BL5	0.4	0.0026	0.00027	136	79959	1.79	-

layers are small enough, under ordinary conditions, to generate laminar boundary layers, in the present they are strongly perturbed into early transition by the high free stream turbulence intensities. The transitional boundary layers were induced in order to provide a better test for the LVG measurements.

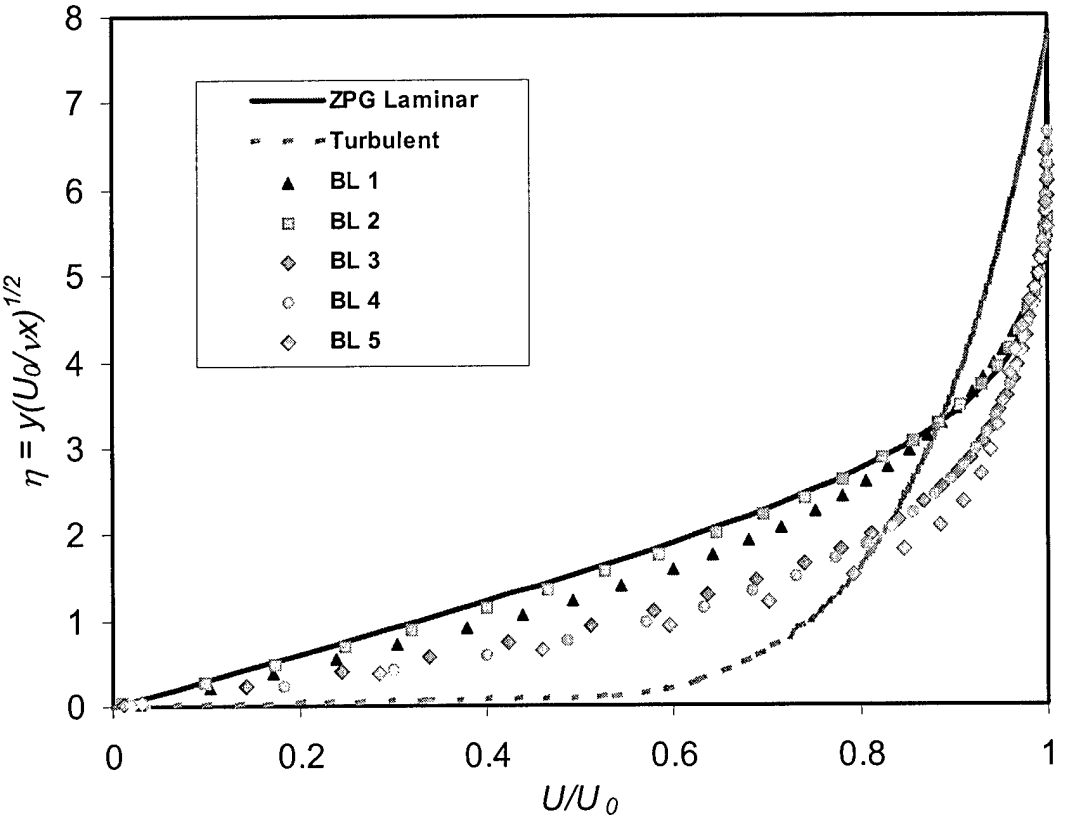

Figure 31: Normalized mean velocity profiles

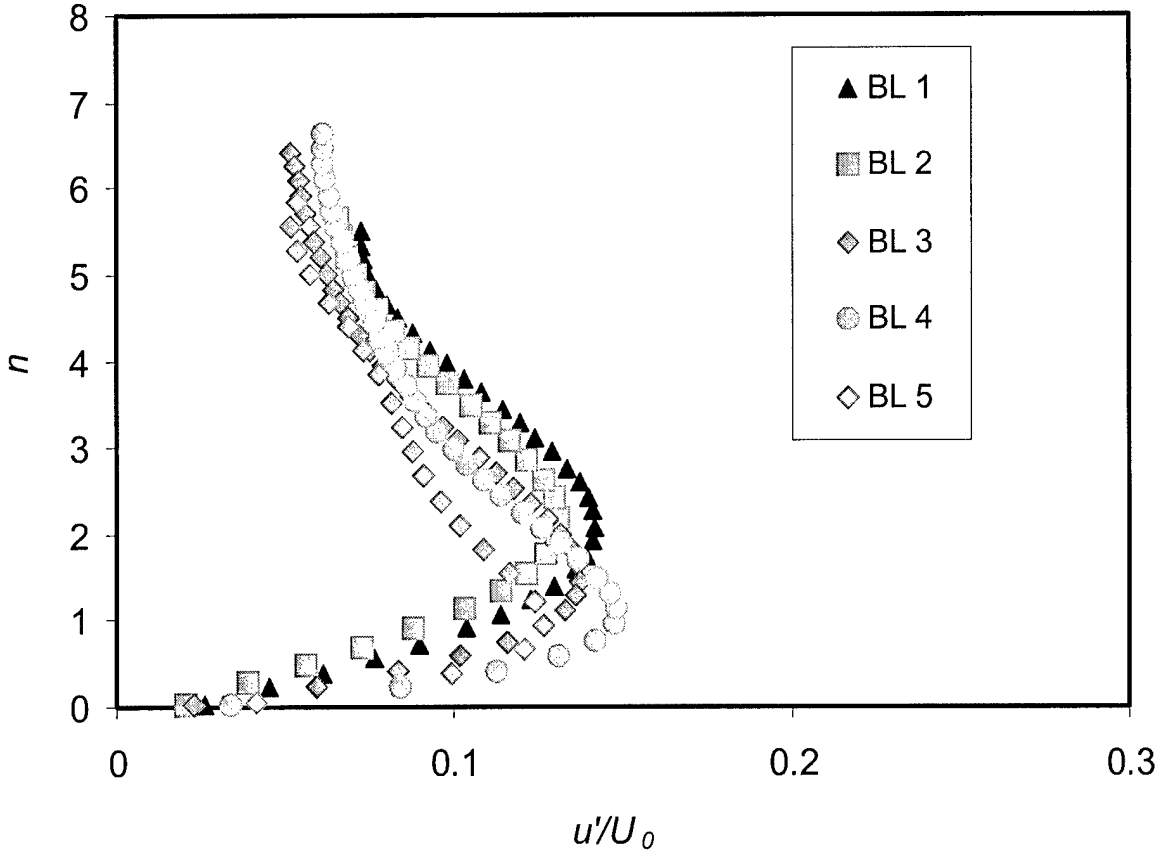

Figure 32: Turbulence intensity profiles

Figure 31 shows the mean streamwise velocity profiles for the five boundary layers studied. The velocity profiles were obtained by the LDV system. The Blasius profile for the zero pressure gradient (ZPG) laminar boundary layer and the $1/7^{th}$ power law profile for the turbulent boundary layer are also shown in the same figure for comparison. As mentioned above, since Re_x in all cases is between 28000 and 80000, the first conclusion one might draw regarding the boundary layer type would be that they are laminar. However, with the exception of BL2, each profile diverges significantly from the Blasius. Although it might be argued that this divergence is caused by the favorable pressure gradient that was present in each case, the shape factor, H, falls within the laminar range of 2.25-3.5 (Holstein and Bohlen, 1940) only for BL2 and BL3 cases. All other boundary layers, including BL1 with the lowest free stream velocity of U_0 = 14 cm/s, fall outside of this shape factor range. The corresponding boundary layer turbulence intensity profiles shown in Fig 32 also confirm the state of the boundary layers. The free stream turbulence intensities of ~ 5.5% lead to boundary layer maximum turbulence intensities between 12 and 14 %.

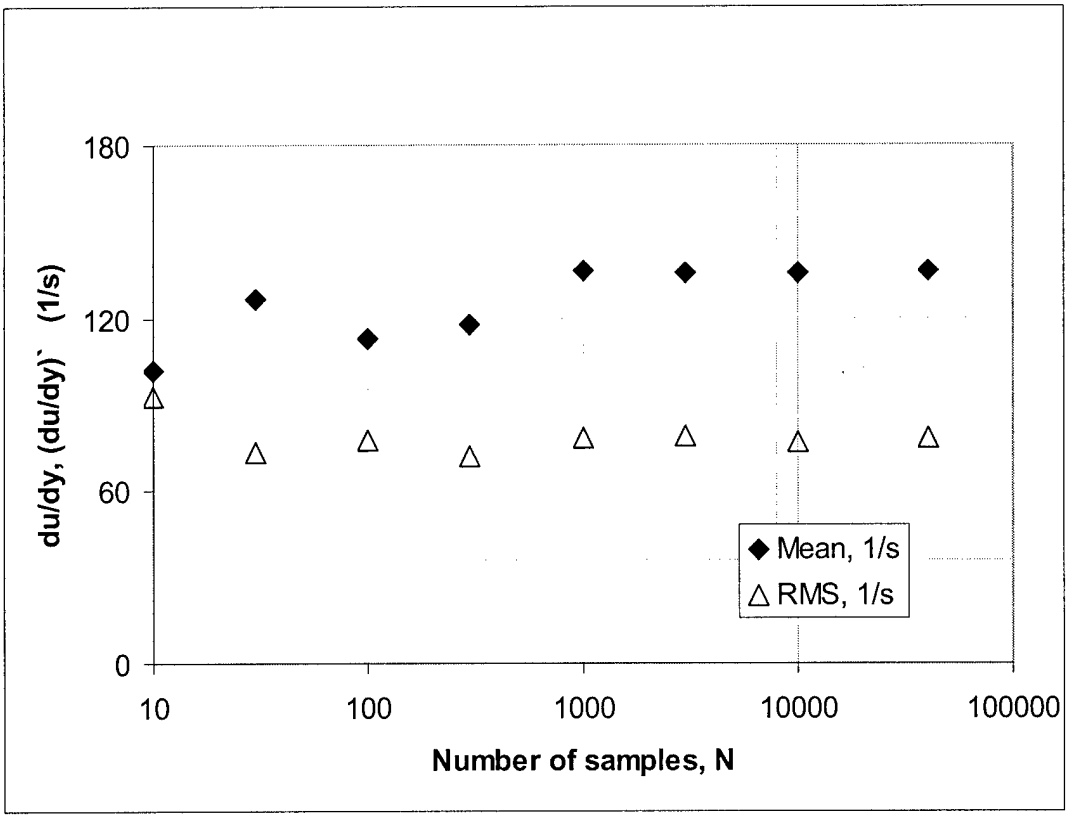

Figure 33: Effect of sampling length on mean and turbulent velocity gradient

Before carrying out systematic measurements of the mean and turbulent vecloity gradient profiles, the influence of sampling record length on velocity gradient statistics was investigated. When the sampling records (or durations) are too short, statistically stationary, unbiased results may not be achieved. To investigate this and to ensure that the results are free of such bias, we made systematic measurements for the effect of record length on mean and turbulent velocity gradients at various boundary layers and locations. A sample is given in Fig. 33 where the effect of sample size, N, on the mean and turbulent velocity gradient for BL 5 at y = 1 mm is presented. The data rate for these measurements was ~ 50 Hz. In this case, for N > 1000 both quantities settle to their respective statistically stationary values. Thus, in the results that will be shown next, measurements were carried out, for each case, with N much larger that the minimum value (typically, 5000 or larger).

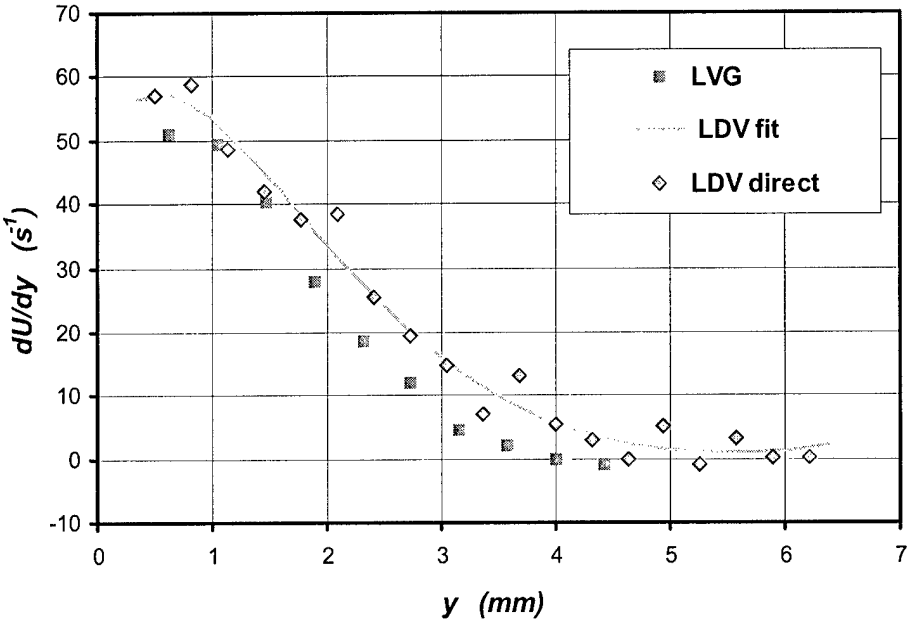

Figure 34: Comparison of velocity gradients obtained from LDV profiles and the LVG probe for BL 1

The mean velocity gradient profiles for BL1 are shown in Fig 34. In addition to the LVG measurements, profiles of mean velocity gradient inferred form the LDV measurements are shown in the figure. The probe separation distance for the LVG measurement is dy = 770 μm. The profile obtained using the mean velocity profiles from LDV data show significantly more scatter when compared to the LVG results, clearly demonstrating the reduced uncertainty in this direct measurement. The additional curve in Fig 34 is obtained by first fitting the LDV velocity profile with a smooth function and then taking the derivative of this function. The agreement between the LDV fit and the LVG data is quite good although, on average, LVG data is slightly lower. The mean velocity gradients for BL2 and BL3 are shown in Fig 35. Again, for the LVG measurements, the probe separation distance is dy = 770 μm. In this figure, in addition to the LDV fit, velocity gradient values obtained by using the finite difference of LDV fit data corresponding to the locations of the two spots of the LVG are also presented to make a more direct comparison between the two types of measurements. Again, the qualitative agreement between the LDV and LVG data is quite good although LDV data is slightly but consistently larger than that for LVG.

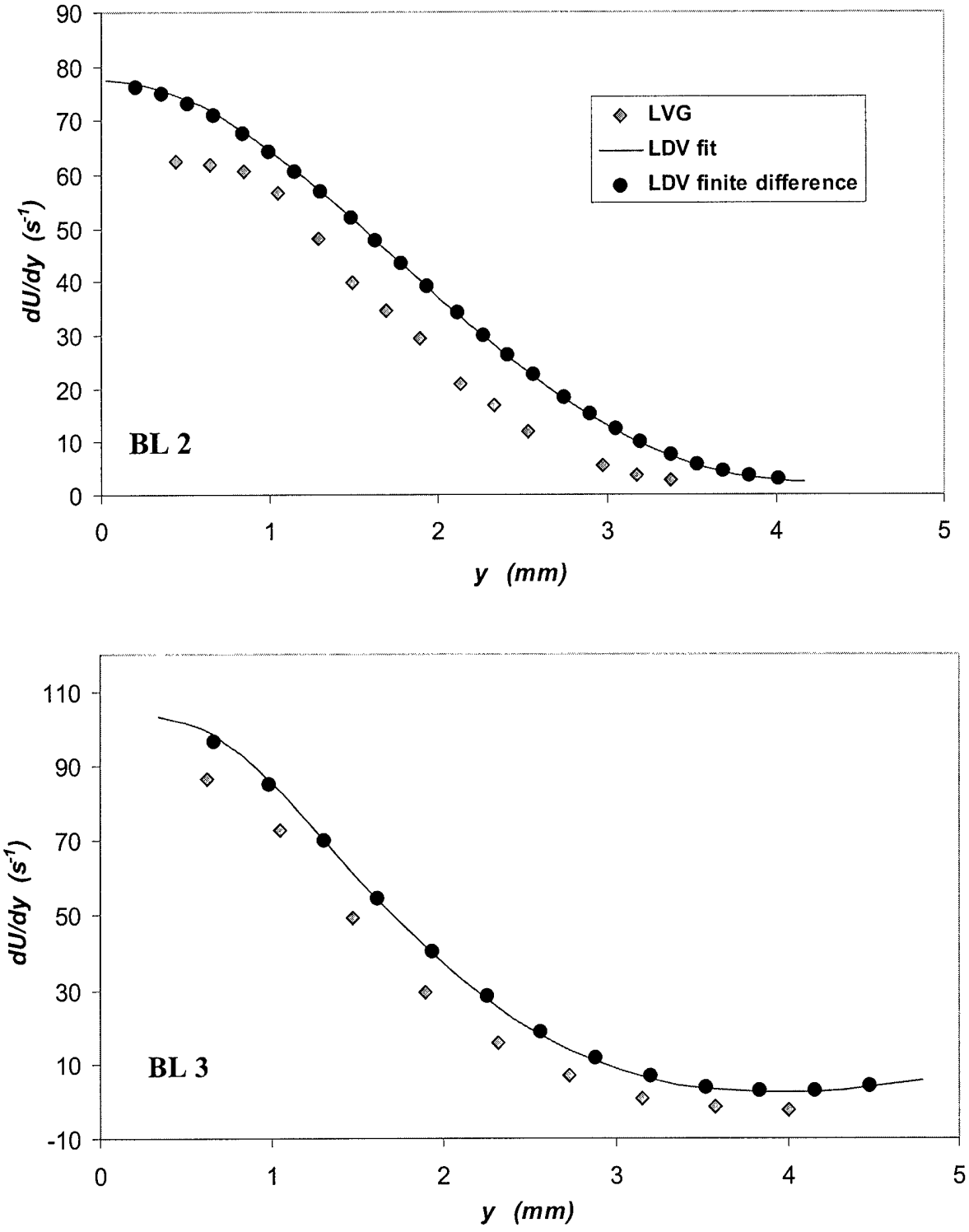

Figure 35: Mean velocity gradient profiles for BL 2 and BL 3

Figures 36 and 37 show the mean velocity gradient profiles for BL4 and BL5, respectively. For each case, two sets of LVG measurements were made; one with dy = 770 μm and another with dy = 300 μm. As before, the mean velocity gradients for the LDV profiles were calculated by first fitting the velocity data by smooth functions in order to reduce the scatter in the profiles. The figures indicate that the probe separation distance, dy does not have a significant influence on the LVG profiles for either boundary layer. The agreement between the LVG and LDV profiles is generally strong. The agreement is particularly good for the BL5 case with the exception of the region very near the wall. Adjacent to the wall, the LVG profiles with dy = 300 μm exhibit a positive slope. It is unlikely that this sudden change in the slope for the LVG profiles represents actual flow physics. Rather, it can be explained by the fact that, very close to the wall (y < 300 μm), one of the probe spots starts hitting the Plexiglas wall. The laser light scattered from the wall is still captured by the collecting optics and is heterodyned with the signal form the other spot in the actual flow. This effectively reduces the dy of the probe and hence, results in the underestimation of the velocity gradient. Therefore, the LVG measurements in this region are not valid since the y distance is essentially smaller than the effective probe size.

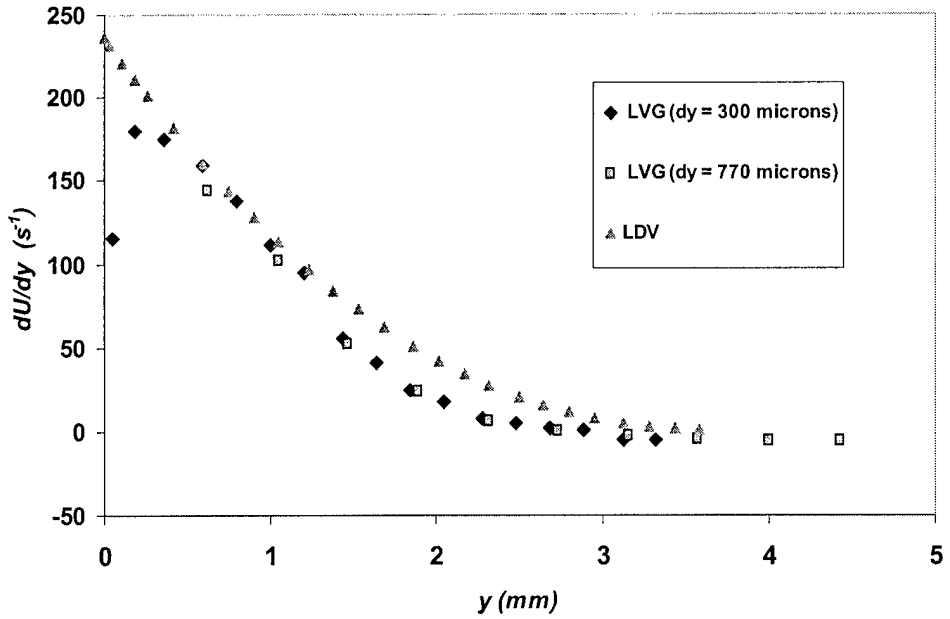

Figure 36: Mean velocity gradient profile for BL 4

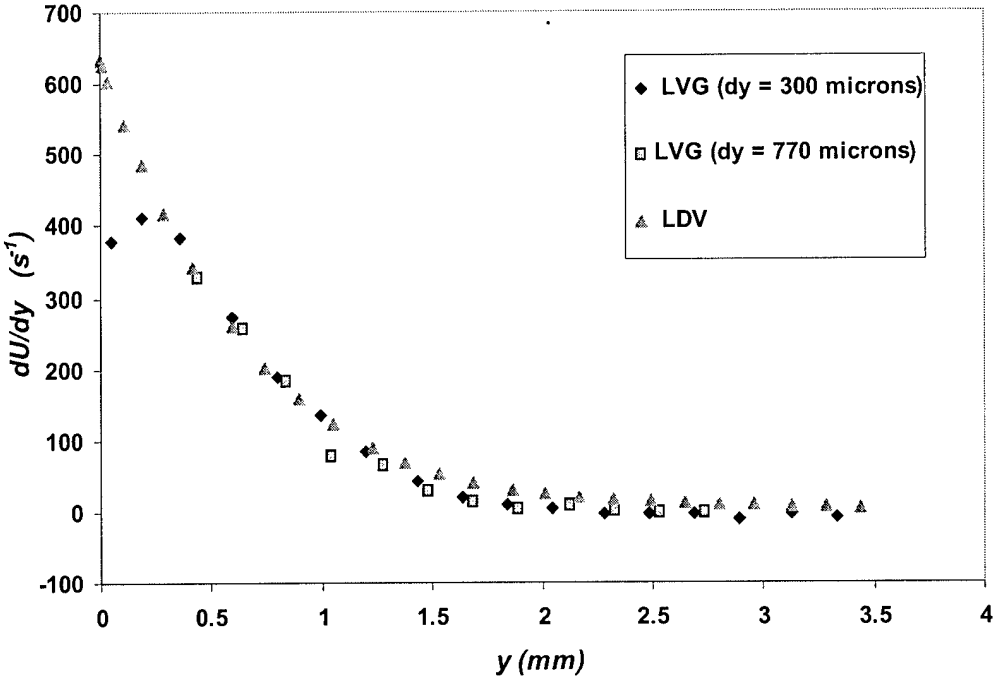

Figure 37: Mean velocity gradient for BL 5

Figure 38 shows the rms of the fluctuating component of velocity gradient for boundary layers BL 4 and BL 5. These are obtained using the LVG probe with dy = 300 μm. Boundary layer BL5, which has the higher free stream velocity and the average velocity gradient exhibits generally higher *(du/dy)'*. For this boundary layer, a maximum value of 125 s^{-1} is reached around $y \approx 0.4$ mm. The distribution for BL4, on the other hand, is rather flat with no discernable peak. (However, it should be pointed out, again, that the data for $y < 300$ μm is likely to be biased as one of the probe spots already hit the wall). A simple analysis shows that the fluctuating velocity difference measurements by the LVG can be related to the turbulence intensity measurements obtained by the LDV through

$$(du')^2 = \left(u_1'^2 + u_2'^2\right) - 2 < u_1 u_2 > .$$

Here, $(du')^2$ is the mean square of the fluctuating velocity difference obtained by the LVG probe while $u_1'^2$ and $u_2'^2$ are the mean square of velocity fluctuations obtained by the LDV at the probe spots 1 and 2 of the LVG. In the last cross correlation term, the symbol <> denotes time averaging. For very large LVG probe spot separation distances, the cross-correlation term, $<u_1 u_2>$ vanishes. In the opposite extreme when $dy \rightarrow 0$, $2 < u_1 u_2 > / \left(u_1'^2 + u_2'^2\right) \rightarrow$ -1. Therefore the above comparison provides a good indication of the spatial resolution of the LVG probe relative to the flow structure. Figure 39 provides one such comparison for BL5 with dy = 300 μm. Here, $(du')^2$ and

$(u_1'^2 + u_2'^2)$ are directly measured by LVG and LDV, respectively while the correlation $\langle u_1 u_2 \rangle$ is calculated from those measurements. The correlation reaches a maximum of about 0.002 cm^2/m^2 at $y \approx 0.8$ mm.

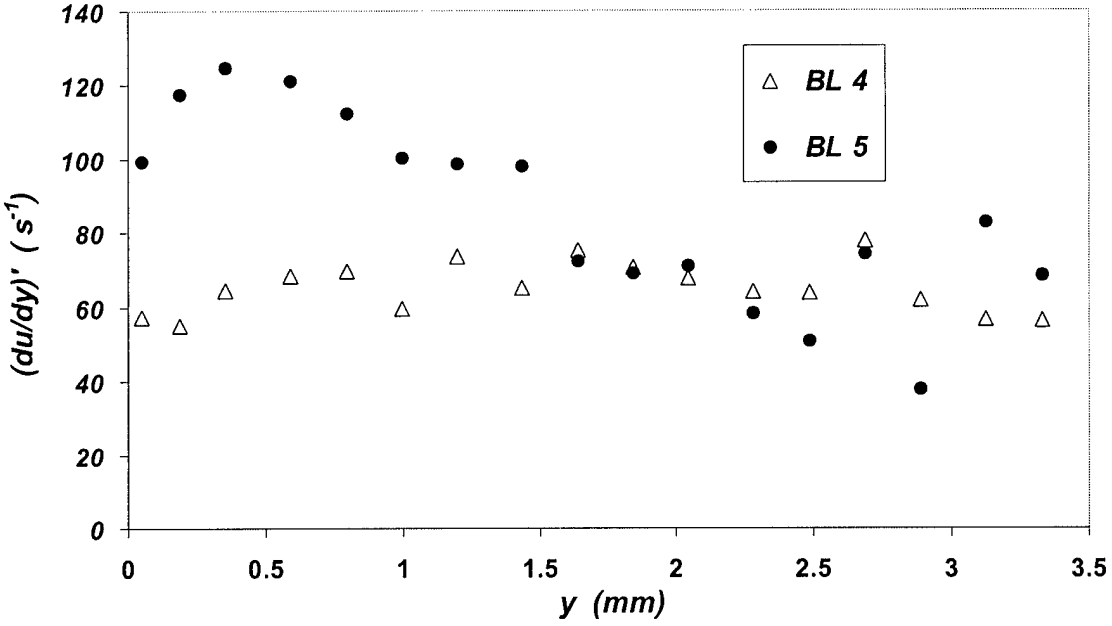

Figure 38: Profiles of RMS velocity gradient for BL 4 and BL 5

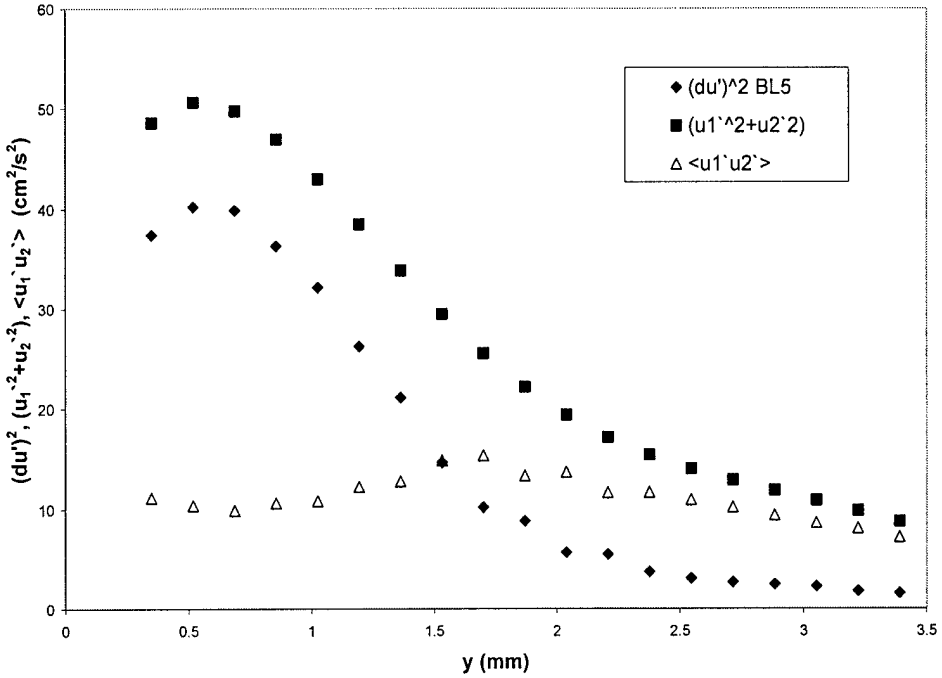

Figure 39: Comparison of fluctuating velocity gradient to turbulence intensity

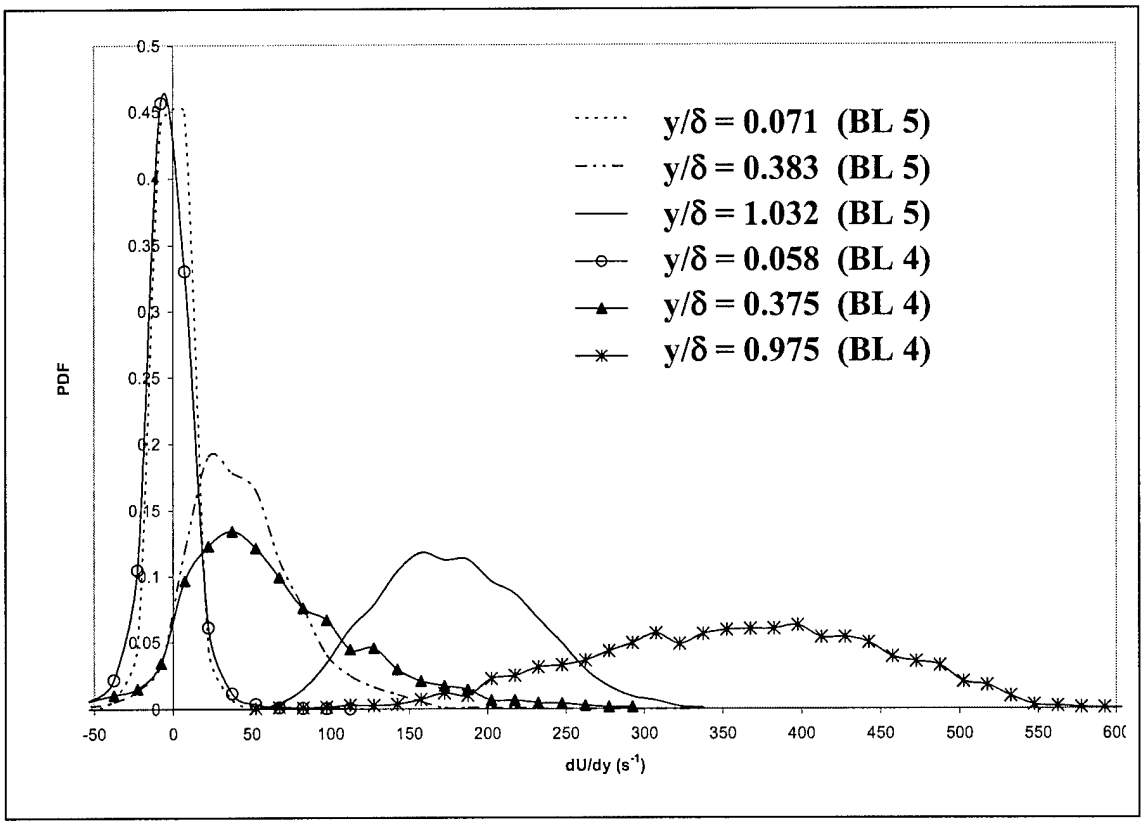

Figure 40: Probability density distributions of the velocity gradient for BL 4 and BL 5

Figure 40 presents the pdf distributions of the velocity gradient for the boundary layers BL4 and BL5, again, using the LVG probe with $\Delta y = 300$ μm. At the outer edge of the boundary layers near the free steam, the pdf distributions are narrow and symmetric. As the wall is approached, the distributions become progressively wider and become slightly skewed.

7.2. Turbulent Boundary Layers

Turbulent boundary layer LVG and LVP measurements were made in the boundary layer facility. Several velocity gradient components were obtained which include, $\partial u/\partial y$, $\partial v/\partial x$, $\partial v/\partial y$. From long records (typically > 2000) of the time-frozen measurements, the profiles of mean and turbulent velocity gradients were obtained in addition to the probability density function distributions (pdf). The spanwise component of the vorticity was also measured. A number of Reynolds numbers and streamwise pressure gradients were considered. In the following, the results for only two representative turbulent boundary layers (TBL) will be presented for the sake of brevity.

Table 5: Characteristics of the turbulent boundary layers studied

	U_0 (m/s)	Re_x	Re_θ	δ (mm)	δ_1(mm)	θ (mm)	H	Λ ($x10^{-8}$)
TBL 1	1.20	$2.17x10^6$	2480	17.27	2.13	1.66	1.28	3.07
TBL 2	0.71	$1.28x10^6$	1830	21.08	2.62	2.07	1.26	6.04

The momentum thickness-based Reynolds numbers for the two boundary layers presented here are Re_θ = 2480 and 1830. Since the test section wall is Plexiglas, these boundary layers developed over "smooth" surfaces. The detailed characteristics of the two boundary layers are given in Table 5. Here, U_0, δ, δ_1, θ and H are the free stream velocity, delta thickness, displacement thickness, momentum thickness and the shape

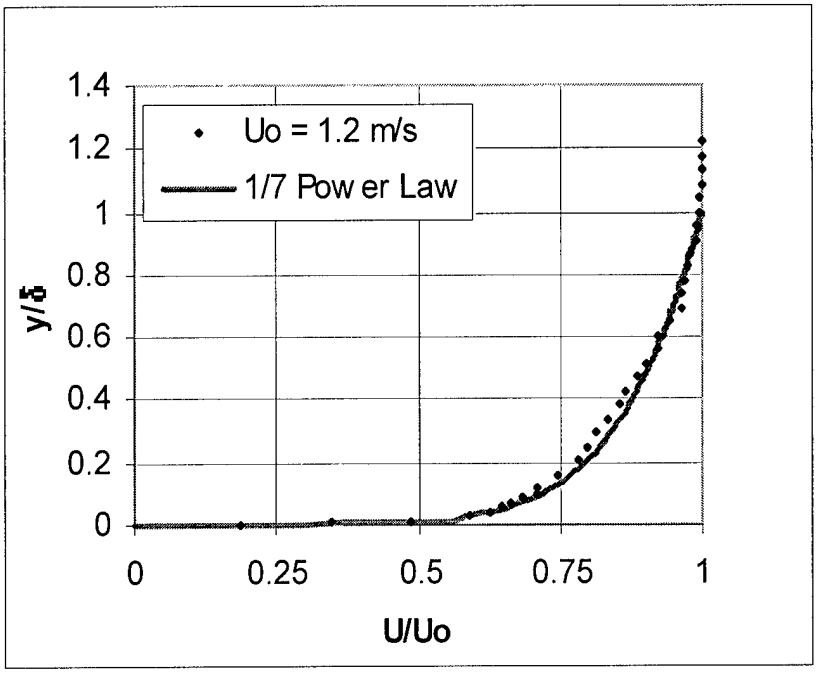

Figure 41: Mean velocity profile for TBL1 plotted using outer layer parameters

factor, respectively. The values for the pressure coefficient, $\Lambda = -(dP/dx)(\delta^2/\mu U_0)$, indicate that the streamwise pressure gradient is nearly zero for both TBLs. This is also evident in the shape factor values for both cases.

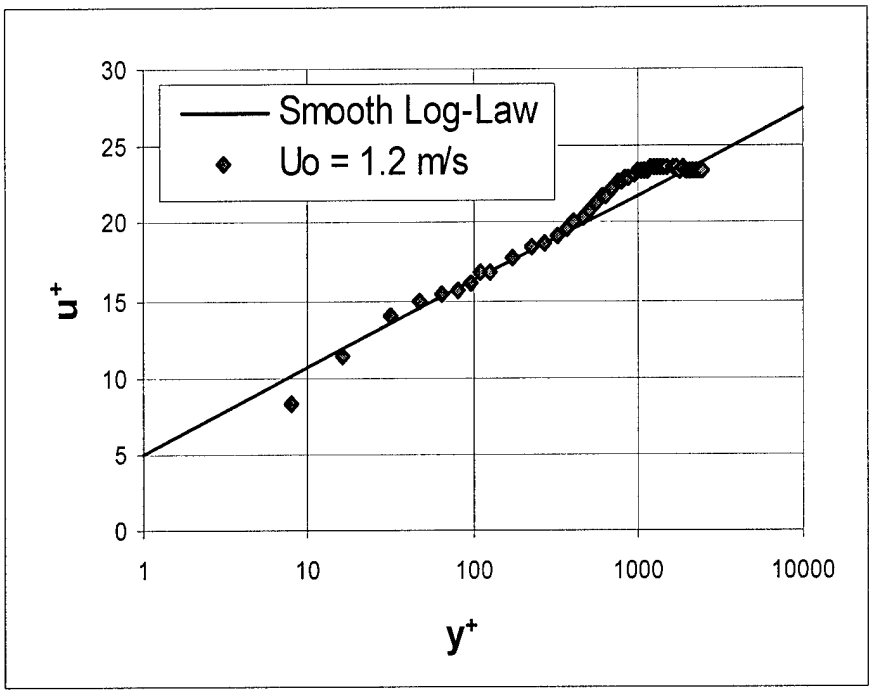

Figure 42: Mean velocity profile for TBL1 plotted using inner layer parameters

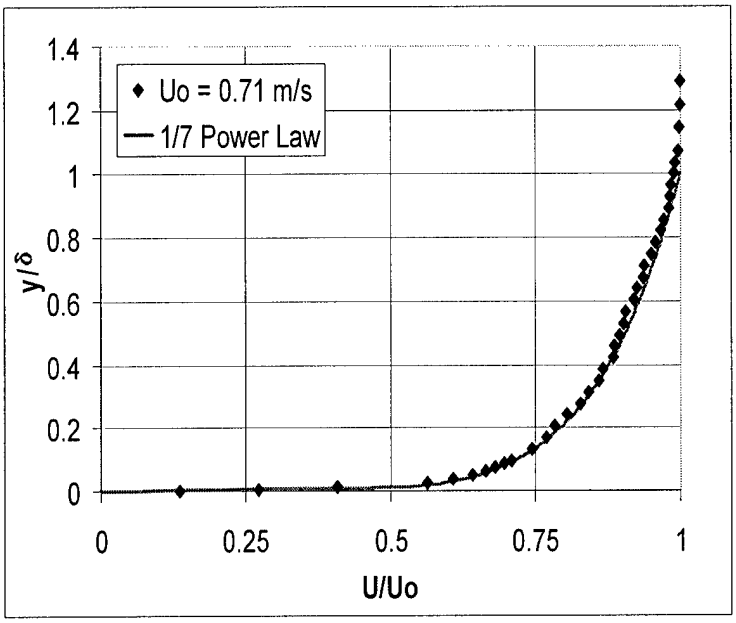

Figure 43: Mean velocity profile for TBL2 plotted using outer layer parameters

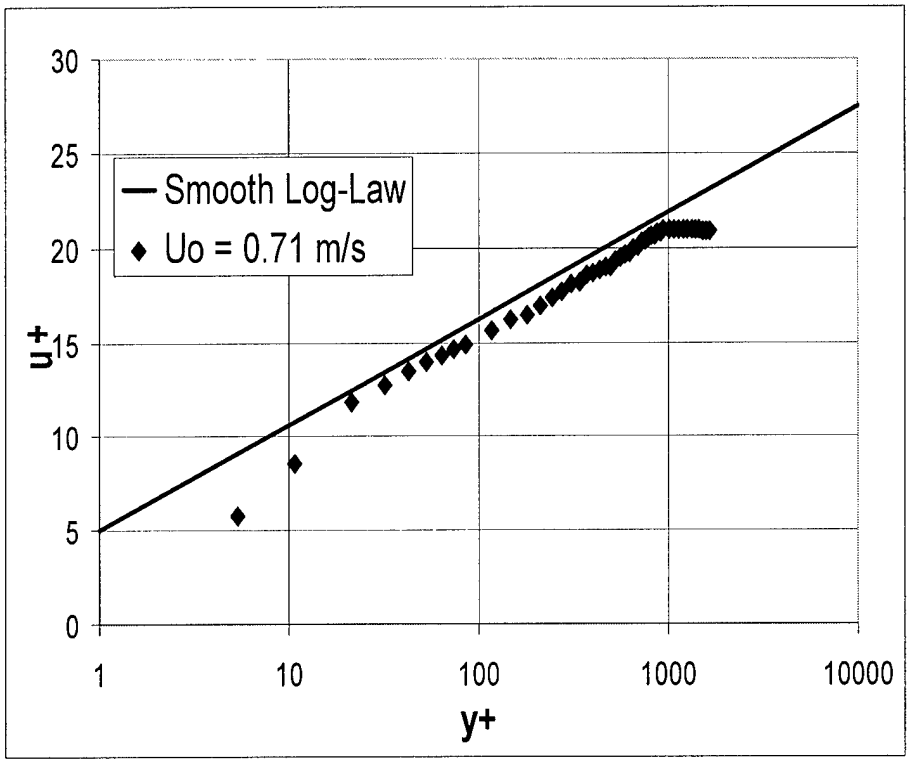

Figure 44: Mean velocity profile for TBL2 plotted using inner layer parameter

Figures 41 and 42 show the mean velocity profile for TBL1 normalized using outer layer and inner layer parameters, respectively. The same is presented for TBL2 in Figs 43 and 44. In Figs. 41 and 43, $1/7^{th}$ power law profiles are also shown for comparison. In Figures 42 and 44, the log-law distribution for a TBL on a smooth wall is also presented for comparison. The outer layer is well represented by the1/7th power law while the near-

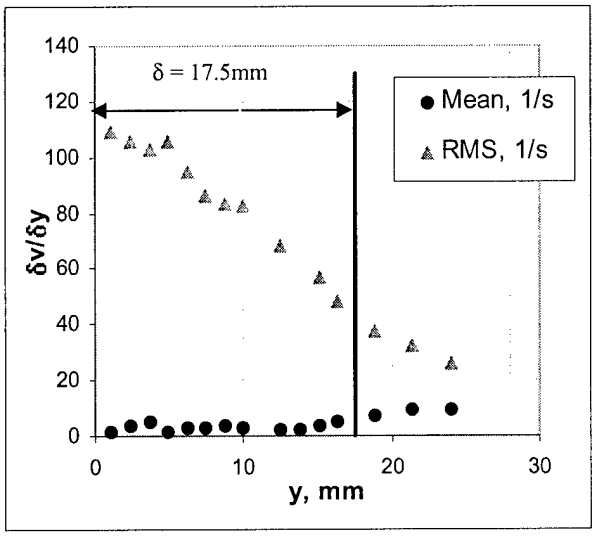

Figure 45: Mean and rms profiles of $\partial v/\partial y$ measurements

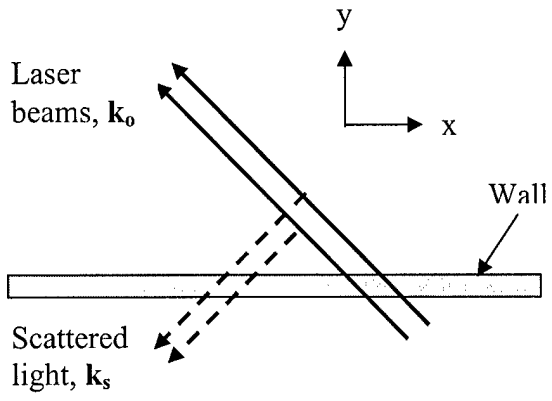

Figure 46: Configuration for $\partial v/\partial y$ measurements

wall region is fit very well to the smooth wall log-law. (Note that the wall shear stress was determined using Clauser's method). Both TBLs are under a mild FPG as can be seen in the up-curving near the outer edge, particularly in Fig 42 for TBL1.

The mean and rms $\partial v/\partial y$ profiles for TBL1 are shown in Fig. 45. These profiles were obtained using the LVG probe configured similar to that described in Fig. As before, the probe is driven by the Ar+ laser and a single 50μm core diameter fiber is used on the signal collection side. As shown in Fig. 46, the optical system is oriented such that both the laser beams forming the probe spots and the collecting optics receiving the Mie scattered signal are on the same side of the wall. This is the prototype of the wall sensor. In the near future, in collaboration with Viosense Inc., we plan to develop a compact version of this sensor using diffractive optical elements that can be built to measure either $\partial v/\partial y$ or $\partial v/\partial x$ and $\partial v/\partial z$. The separation distance, dy in the present experiment is 700 μm. Each data point in Fig. 45 represents a record length ranging between 1000 and 2000 individual realizations. The rms of the velocity gradient increases monotonically towards the wall with the highest value of 110 Hz obtained closest to the wall (y = 1.1 mm). This result is consistent with previous measurements of the rms of wall normal velocity, v', which show an increase towards the wall (in the outer layer). An order of magnitude analysis using the available v' data also shows that the values obtained are quite reasonable. Unfortunately, there are no other direct measurements available with which we could compare the present results. The mean values of $\partial V/\partial y$ are very small and the profile does not seem to follow a trend. We suspect that this is at least partially due to the very small values of the transverse velocity in the boundary layer, which makes the

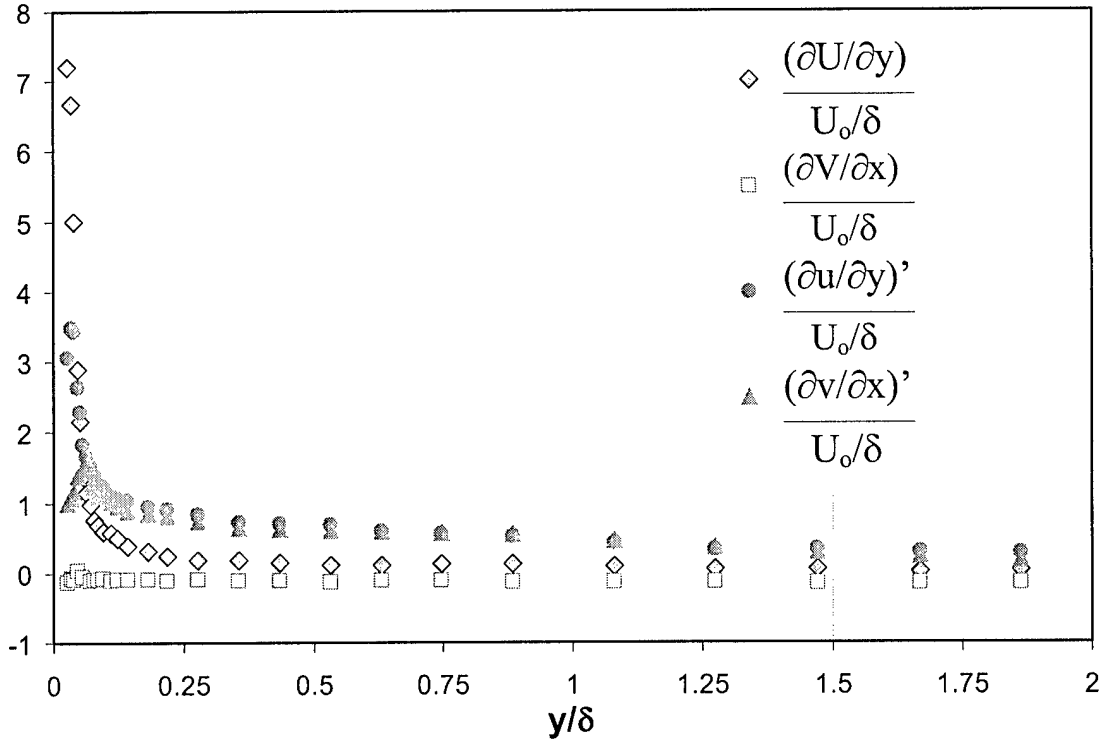

Figure 47: Mean and rms profiles of $\partial u/\partial y$ and $\partial v/\partial x$ (TBL 1)

measurement of the gradients quite challenging. We have not carried out direct measurement of the transverse velocity but typical estimated values are in the order of several mm/s for the present boundary layer. Therefore, with the given separation distance, *dy* for the probe, typical mean velocity differences are in the order of several hundred μm/s. Although the current optical configuration and electronics provide a resolution of ~ 35 μm/s, measurement of such small velocity differences is still a challenge.

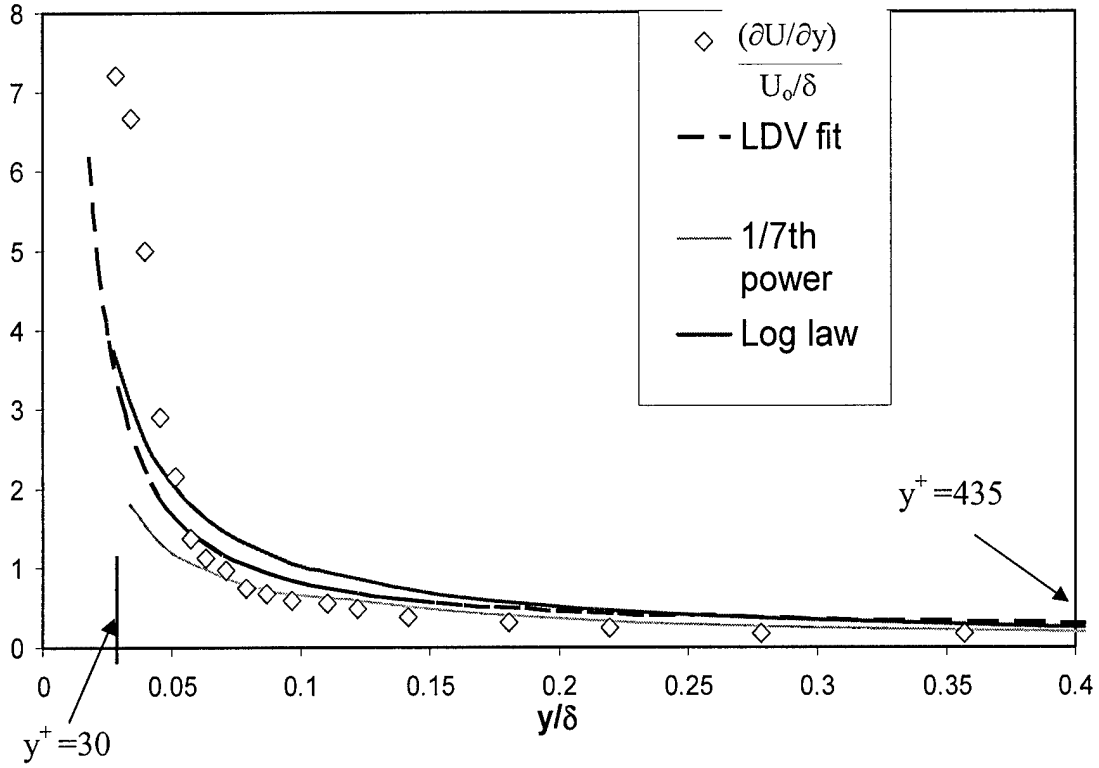

Figure 48: Near wall profile of $\partial U/\partial y$ (TBL 1)

In the ∂u/∂x and ∂v/∂y measurements, the optics are set up as LVP (as shown in Figs. 9 and 10) so that both gradients are measured simultaneously. The separation distances for the gradient measurements were dx = 300 ±10 μm and dy = 770 ±10 μm. The diameter of the two laser beams at the probe area was ~ 150 μm. each laser beam had a power of about 75 mW at the probe location. The data rate for each gradient measurement was in the range of 10 to 15 Hz. Record lengths of 3000-500 were used to calculate the mean and rms of the velocity gradients. For vorticity, the data rate was 0.2-0.6 Hz (90-300 samples) for a coincidence time window of 1 ms and 1.6-3.0 Hz (700-1400 samples) for a coincidence window of 10 ms.

Figure 47 shows the mean and rms profiles of $\partial u/\partial x$ and $\partial v/\partial y$ for TBL1. The gradients are normalized using the free stream velocity and the boundary layer thickness, δ. The mean transverse gradient of the streamwise velocity grows rapidly as the wall is approached whereas the mean streamwise gradient of the transverse velocity is essentially flat throughout indicating the comparatively small values of this gradient. On the other hand, the rms of the gradient of transverse velocity is significant, showing a peak of about 1.5 near the wall. Still, the rms of $\partial u/\partial y$ is dominant with a peak value of ~ 3.5. Figure 38 shows the near wall behavior of the transverse gradient of streamwise velocity. For comparison, the mean velocity gradient obtained from the LDV velocity measurements as well as the power law and log-law (for smooth surfaces) are also shown in the same figure. The distances in wall units are also indicted at two locations. (Note that for BL1 one wall unit is $y^+ \approx 16$ μm). The agreement among the data and the models are good in the outer portion of the wall region. Closer to the wall, the model fits and the measured data start to diverge with the LVG results giving the larges mean gradient values.

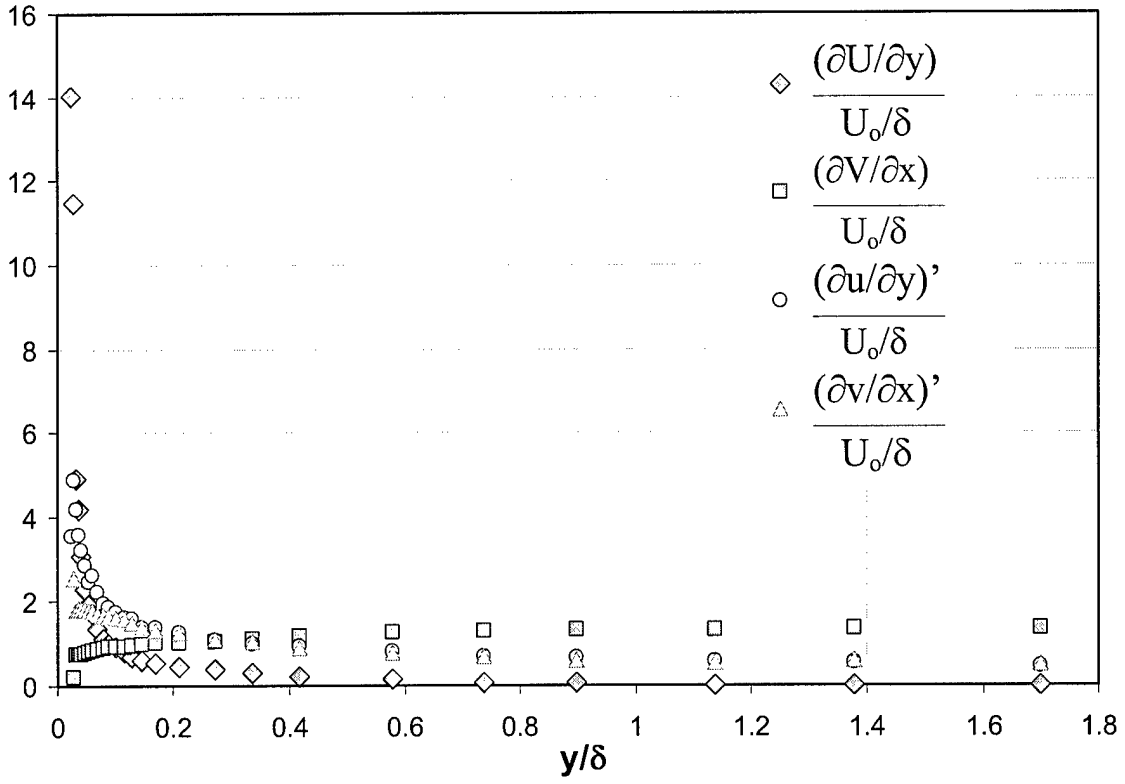

Figure 49: Mean and rms profiles of $\partial u/\partial y$ and $\partial v/\partial x$ (TBL 2)

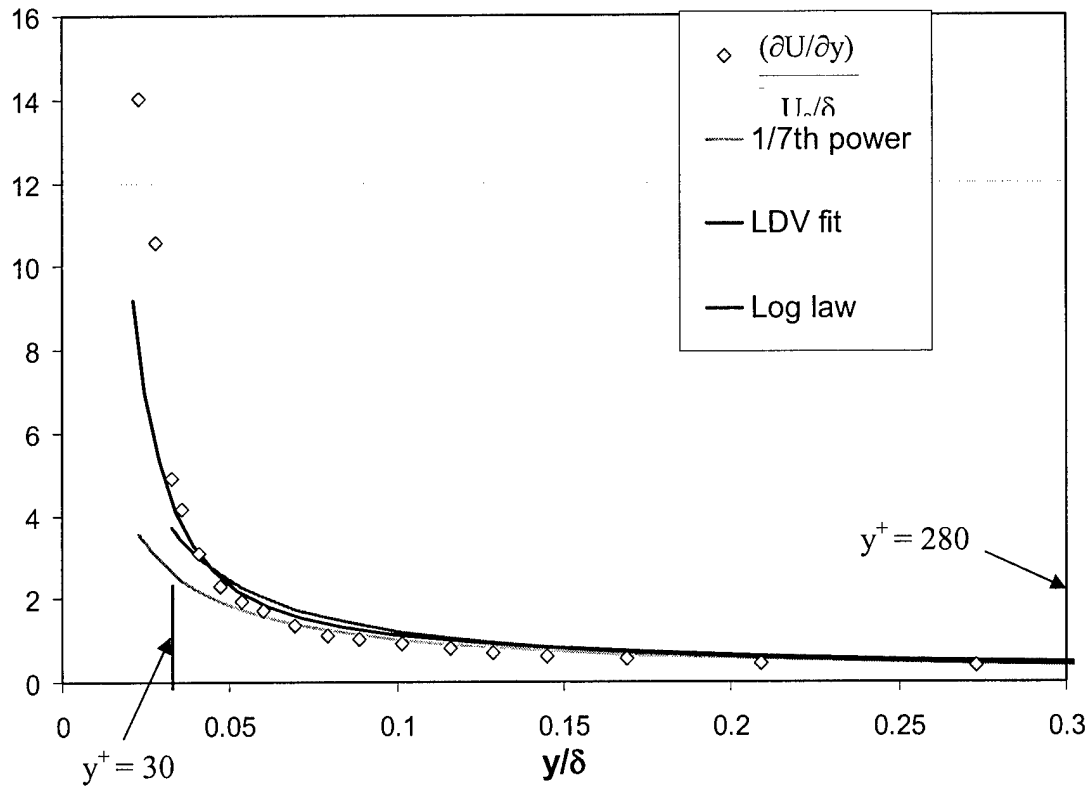

Figure 50: Near wall profile of $\partial U/\partial y$ (TBL 2)

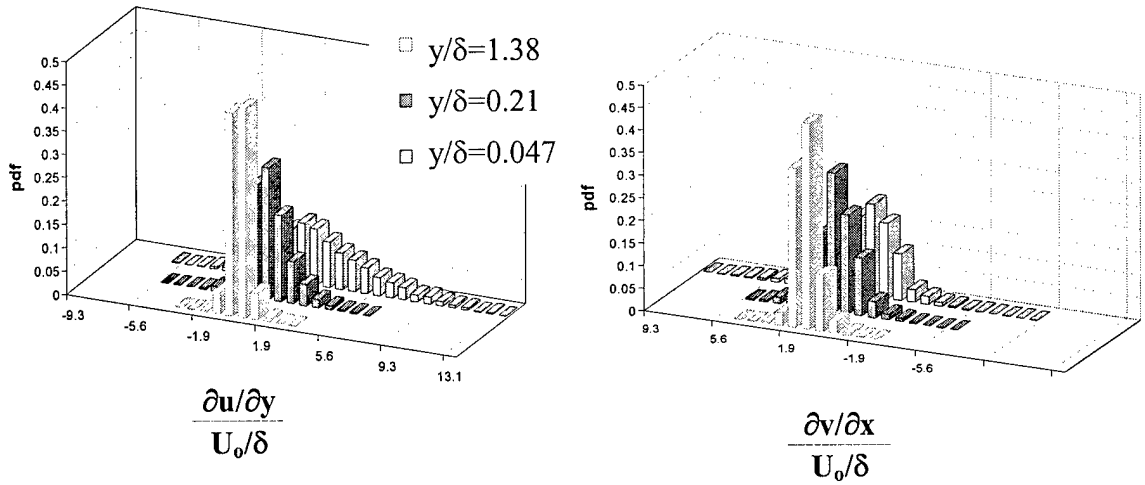

Figure 51: Pdf of $\partial u/\partial y$ and $\partial v/\partial x$ (BL 2)

Figures 49 and 50 show the same profiles for TBL2. For this boundary layer, one wall unit is $y^+ \approx 19$ μm. Again, the agreement among the measured data and the power-law and log-law models is very good for $y^+ > 70$. As expected, the power law starts diverging significantly for $y^+ < 50$. Closer to the wall ($y^+ < 35$), the log-law also diverges from the measured data as the laminar sublayer is approached. Nevertheless, the LVG measurements clearly indicate the viability of this new technique for turbulent boundary layers.

The probability density distributions of $\partial u/\partial y$ and $\partial v/\partial x$ for TBL2 are shown in Fig. 51. Outside the boundary layer, the pdf distributions of both gradients are narrow. Inside the boundary layer, however, these distributions for both gradients become wider as the wall is approached which is consistent with the increased turbulence near the wall. For all the cases studied, the distributions well represented by a normal function.

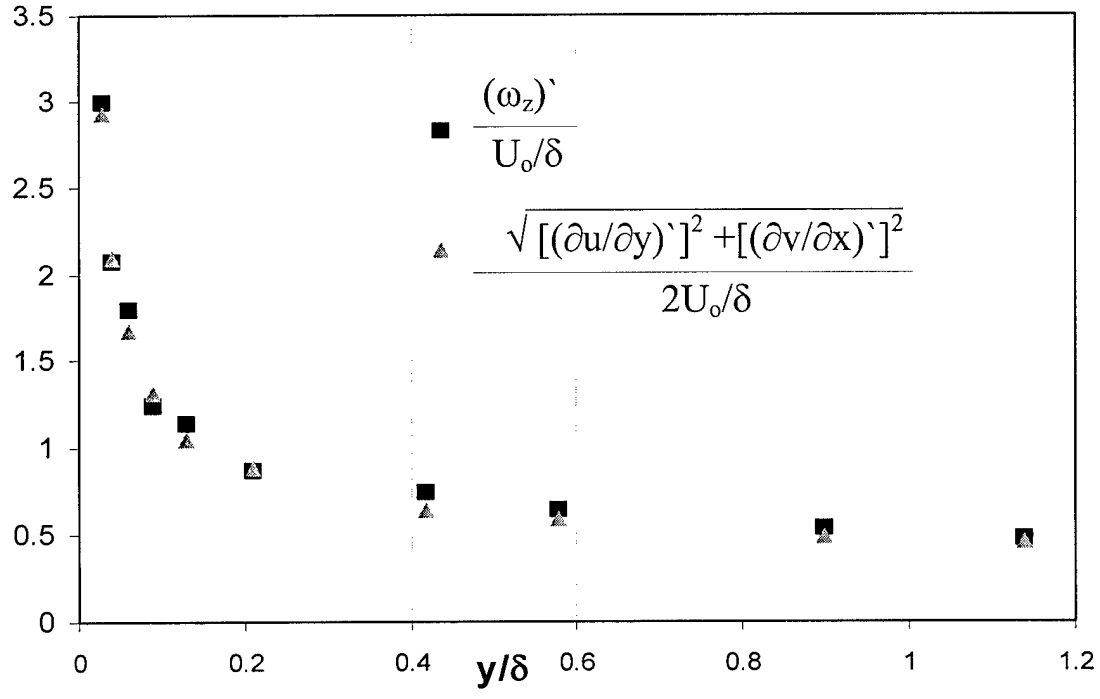

Figure 52: Rms of vorticity component ω_z (BL 2)

In the boundary layer, as we have seen earlier in Figs. 47 and 49, the contribution of mean gradient $\partial V/\partial x$ is negligible to the mean spanwise vorticity and its distribution is essentially the same as that for $\partial U/\partial y$. Therefore, the mean spanwsie vorticity results are not shown here. As for the fluctuating vorticity, a sample is shown in Fig. 52 which presents the rms of the fluctuating spanwise vorticity for TBL2. The rms vorticity is normalized by the free stream velocity and the boundary layers thickness and is represented by the solid squares. As seen, the turbulent vorticity is very small in the outer

portion of the boundary layer but becomes progressively larger as closer to the wall. In A simple analysis shows that

$$\omega_z' = \frac{1}{2}\sqrt{\overline{\left(\frac{\partial v}{\partial x}\right)'^2} + \overline{\left(\frac{\partial u}{\partial y}\right)'^2} - 2\overline{\left(\frac{\partial v}{\partial x}\right)'\left(\frac{\partial u}{\partial y}\right)'}}$$

That is, the mean square of fluctuating vortricity is proportional to the sum of the mean square of the two fluctuating velocity gradients plus a cross correlation of the gradients as shown in the last term of the above equation. In order to assess the influence of this cross correlation term, the square root of sum of the two mean squares of two fluctuating gradients have also been plotted in the figure (triangle symbol). Surprisingly, the two profiles agree very well with each other indicating that the cross correlation term is essentially inconsequential. The same has been done for different boundary layers with similar results.

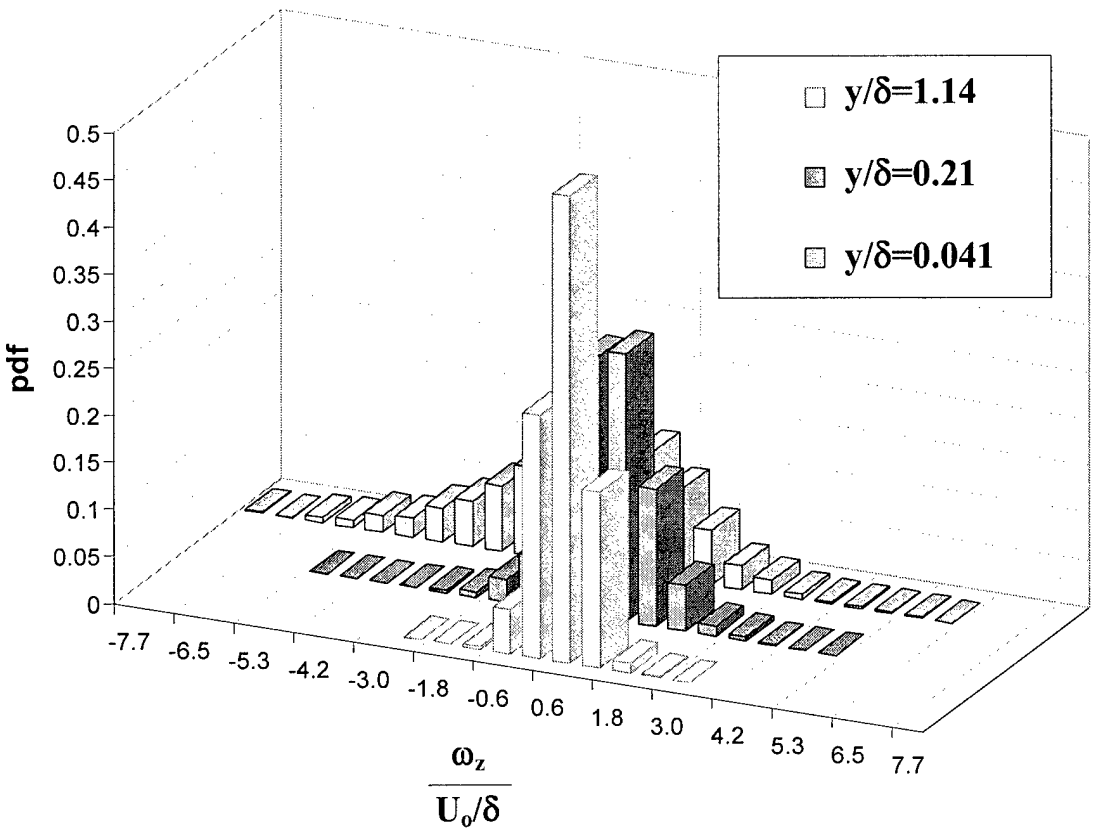

Figure 53: Pdf of ω_z for TBL2

The probability density function distributions of the spanwsie vorticity at three locations for TBL2 are shown in Fig. 53. These distributions are similar to those for the velocity gradients as would be expected.

8. CONCLUSIONS

A novel laser-based velocity gradient and vorticity measurement technique has been developed and demonstrated in several types of water flows. Measurements were made in turbulent two-stream mixing layers as well as transitional and turbulent boundary layers. These measurements have clearly shown the viability of the laser LVG and LVP techniques as a research tool in shear flows. The mean gradient results were compared to those calculated from mean velocity profiles obtained by LDV measurements that were carried out simultaneously and very good agreement was found between the two sets of results for both mixing layers and boundary layers. Although in the present project, no measurements were performed in gas flows, there is no principle that could prevent the application of this measurement method to gas flows. The technique is attractive since it measures the velocity gradient directly without having to measure velocity first at two locations. It can provide spatially well-resolved, time-frozen measurements. The optical set up is relatively simple and inexpensive and can be assembled using mostly off-the-shelf components. Since the heterodyne signal is similar to the Doppler signal of the LDV method, the same signal processing electronics are used which further makes the technique attractive. In addition to its utility as a fluid mechanics research tool, the LVG principle can be exploited to build miniaturized, wall-mounted sensors for use in fluid dynamic systems to detect instability (or turbulent event) or separation. Such wall sensors could potentially be used as distributed sensors for active flow control.

Certain considerations need to be taken into account when applying the technique in fluid mechanics. First of all, it is a technique that requires particles to scatter the incident laser light, as in the well known LDV method. However, in order to realize the heterodyne signal, particles must occur in each of the two spots of the probe volume simultaneously; it is a two particle scattering process rather than one (as in LDV). Therefore, for similar data rates, higher seed densities (or loadings) will be needed. On the other hand, if too many particles exist in each probe spot, the coherence of the scattered light will be corrupted leading to poor heterodyne. The analysis presented in Section 5.1 provides the seed density requirements and expected data rates as a function of optical parameters and flow velocity.

In order to achieve heterodyne with a robust beat signal, the Mie scattered light from the two measurement spots of the LVG have to be made collinear before it is focused on the photo detector. The angle, α, between the two incoming signals incident on the detector have to fulfill the criterion $d \geq \lambda/[2\mathrm{Sin}(\alpha/2)]$, where d is the focused spot size on the detector and λ is the laser wavelength. This is a fairly stringent requirement that makes the optical alignment quite challenging. We have found that the most practical approach is to couple the signals into two optical fibers and then join them using a beam splitter in reverse that is built into the optical fibers. These optical fiber elements are readily available for a range of laser wavelengths since they have applications in the telecommunication industry. In the future LVG sensors, can be made compact and rugged by using diffractive optical elements. This would also simplify the alignment procedure.

9. REFERENCES

Adrian, R.J., "Particle Imaging Techniques for Fluid Mechanics", 1991, *Annual Review of Fluid Mechanics.*, Vol. 20, p. 261.

Agui, H.A. and Andreopoulos, Y., "Development of a New Laser Vorticity Probe-LAVOR", 1994, *Laser Anemometry: Advances and Applications,* Ed. Huang, T.T. and Otugen, M.V., ASME-FED, Vol 191., p.15.

Andreopoulos, Y. and Honkan, A., "Experimental Techniques for Highly-Resolved Measurements of Rotation, Strain and Dissipation-Rate Tensors in Turbulent Flows", 1996, *Measurement Science and Technology*, Vol. 7, p. 1462-1476.

Balint, J-L, Wallace, J.M. and Vukoslavcevic, P, "The Velocity and Vorticity Vector Fields of a Turbulent Boundary Layer. Part 2. Statistical Properties", 1991, *J. Fluid Mech*. Vol. 228, pp.53-86.

Barnhard, D.H., Adrian, R.J. and Papen, G.C., "Phase Conjugate Holographic System for High Resolution Particle Image Velocimetry", 1994, *Appl. Optics* , Vol. 33, No.30, p. 7159.

Breyer,H, Kreigs, H., Schmidt, U. and Staude, W., "The Measurement of Velocity Gradients in Fluid Flow by Laser Light Scattering. Part 1: Mean Gradients", 1993, *Exp. Fluids*, Vol. 15, p. 200.

Eckelmann, H., Nychas, S.G., Brodkey, R.S. and Wallace J.M., " Vorticity and Turbulence Production in Pattern Recognized Turbulent Flow Structures",1977, *Phys. Fluids*, Vol. 20, p. 225.

Foss, J.F. and Haw, R.C., "Vorticity and Velocity Measurements in a 2:1 Mixing Layer", 1990, In *Forum on Turbulent Flows*. Ed. W. W. Bowers and M. Samimy ASME-FED 94, p.115.

Freestone, M.M., "Vorticity Measurement by a Pressure Probe", 1988, *Aeronautical Journal*, Vol. 21, p.29.

Frisch, M.B. and Ferguson, R.D., "Water Compatible Vorticity Vector Optical Probe", 1991, *Proc. Symp. on Turb. Shear Flows, 8th*, Munich, Germany, September 1991.

Frisch, M.B. and Webb, W.W., "Direct Measurement of Vorticity by Optical Probe", 1981, *J. Fluid Mech.*, Vol. 107, pp. 173-200.

Hanson, S.G. "Application of the Laser Gradient Anemometer (LGA) for Fluid Flow Measurements", 2nd *Symposium on the Application of Laser Anemometry to Fluid Mechanics* (Lisbon, 1984)

Hirleman, E. D., "Laser Technique for Simultaneous Particle Size and Velocity Measurements" , 1987, *Optics Letters* Vol. 3, p.p.19

Holstein, H., and Bohlen, T. "Ein einfaches Verfahren zur Berechnung laminarer Reibungsschichten, die dem Naherungsverfahren von K. Pohlhausen genugen" Lilienthal-Bericht S. 10,5-16 (1940)

Huachen, P. and Shiying, Z., "Measurement of Streamwise Vorticity Using a Vane Vorticity Meter", 1987, *Heat and Fluid Flow*, Vol. 8, p.72.

Klewicki, J.C., Falco, R.E. and Foss, J.F., "Some Characteristics of the Vortical Motions in the Outer Region of Turbulent Boundary Layers", 1992, *J. Fluids Engineering*, Vol. 114, p. 530.

Kovasznay, L.S.G., "Turbulence Measurements" In *High Speed Aerodynamics and Jet Propulsion*, 1954. Ed. R.W. Landenbuerg, B. Lewis, R.N. Pease and H.S. Taylor, Vol 9, p. 213.

Kovesznay, L.G.S., Kibens, V. and Blackwelder, R.F., "Large-Scale Motion in the Intermittent Region of a Turbulent Boundary Layer", 1970, *J. Fluid Mech.*, Vol. 41, pp.283-325

Kriegs, H. and Staude, W., "A Laser Pulse Technique for the Measurement of Time Resolved Velocity Gradients in Fluid Flow", 1995, *Measurement Science & Tech*nology, Vol.6, p. 653.

Lang, D.B. and Dimotakis, P., "Measuring Vorticity Using Laser Doppler Velocimetry", 1992, *Bull. AM. Phys. Soc.*, Vol. 27, p. 1166.

Lang, D.B. "Laser Doppler Velocity and Vorticity Measurements in Turbulent Shear Layers", 1985, Ph.D. Thesis, California Inst. Technology, Pasadena, CA.

Meng, H and Hussain, F, "Instantaneous Flow Field in an Unstable Vortex Ring Measured by Holographic Particle Velocimetry", 1995, *Phys. Fluids*, Vol. 7, p. 9

Otugen, M.V. Bivolaru, D. and Arik, E. "PIV Study of a Mach 1.6 Supersonic Jet," *Proceedings of VSJ-SPIE98*, Dec. 1998, Yokohama, Japan.

Otugen, M.V., Su, W-J and Papadopoulos, G. "A New Laser-Based Method for Strain Rate and Vorticity Measurements," 1998, *Measurement Science & Technology* Vol. 9., pp. 267-274.

Vokoslavcevic, P., Wallace, J.M. and Balint, J-L., "The Velocity and Vorticity Vector Fields of a Turbulent Boundary Layer, Part I. Simultaneous Measurement by Hot-Wire Anemometry", 1991, *J. Fluid Mech*. Vol 228, p.25.

Wallace, J.M., Eckelmann, H. and Brodkey, R., "The Wall Region in Turbulen Shear Flow," 972, *J. Fluid Mech.*, Vol. 54, pp. 39-48

Wallace, J.M., and Foss, J.F., "The Measurement of Vorticity in Turbulent Flows", 1995, *Ann. Rev. Fluid Mech.* Vol. 27, p. 469

Wassman W.W. and Wallace, J.M., "Measurement of Vorticity in Turbulent Shear Flows", 1979, *Bull. Am. Phys. Soc.,* Vol. 24, p. 1142.

Wernet, M.P., "Stereo Viewing 3-Component Planar PIV Utilizing Fuzzy Logic Interference", AIAA paper No: 96-2268. (Also, NASA Technical Memorandum TM-107235), 1996.

Wernet, M.P., "PIV for Turbomachinery Applications", SPIE Conf. On Optical Diagnostics in Fluid and Thermal Flow, San Diego, CA, 1997 (Also NASA Technical Memorandum TM-107525)

Yao, S., Tong, P. and Ackerson, B. "Proposal and Testing for a Fiber-Optic-Based Measurement of Flow Vorticity", 2001, *Applied Optics*, Vol. 40, No.24. pp. 4022-4027

Zalay, A.D.,"Hot-Wire and Vorticity Meter Wake Vortex Surveys", 1976, *AIAA Journal*, Vol. 14, p. 694.